

Seasonal and storm event-based dynamics of dissolved organic carbon (DOC) concentration in a Mediterranean headwater catchment

Alfonso Senatore¹, Giuseppina Anna Corrente¹, Eugenio Licio Argento¹, Jessica Castagna¹, Massimo Micieli², GIUSEPPE MENDICINO¹, Amerigo Beneduci¹, and Gianluca Botter³

¹University of Calabria

²University of Padua

³Universita' di Padova

January 9, 2023

Abstract

This study investigates the spatial and temporal dynamics of DOC concentration in a Mediterranean headwater catchment (Turbolo River catchment, southern Italy) equipped with two multi-parameter sondes providing more than two-year (May 2019 to November 2021) continuous high-frequency measurements of several DOC-related parameters. The sondes were installed in two nested sections, a quasi-pristine upstream sub-catchment and a downstream outlet with some anthropogenic disturbances on water quality. DOC estimates were achieved by correcting the fluorescent dissolved organic matter - fDOM - values through an original procedure not requiring extensive laboratory measurements. Then, DOC dynamics at the seasonal and storm event scales were analyzed. At the seasonal scale, results confirmed the climate control on DOC production, with increasing background concentrations in hot and dry summer months. The hydrological regulation proved crucial for DOC mobilization and export, with the top 10th percentile of discharge associated with up to 79% of the total DOC yield. The analysis at the storm scale using flushing and hysteresis indices highlighted substantial differences between the two catchments. In the steeper upstream catchment, the limited capability of preserving hydraulic connection in time with DOC sources determined the prevalence of transport as the limiting factor to DOC export. Downstream, transport- and source-limited processes were observed almost equally. The correlation between the hysteretic behaviour and antecedent precipitation was not linear since the process reverted to transport-limited for high accumulated rainfall values. The study demonstrated the importance of high-resolution measurements to explain DOC dynamics at multiple time scales using a quantitative approach.

Hosted file

953069_0_art_file_10572472_rnmqmq.docx available at <https://authorea.com/users/102313/articles/617662-seasonal-and-storm-event-based-dynamics-of-dissolved-organic-carbon-doc-concentration-in-a-mediterranean-headwater-catchment>

1 **Seasonal and storm event-based dynamics of dissolved organic carbon (DOC)**
2 **concentration in a Mediterranean headwater catchment**

3
4 **Alfonso Senatore¹, Giuseppina A. Corrente², Eugenio L. Argento¹, Jessica Castagna¹,**
5 **Massimo Micieli^{3,1}, Giuseppe Mendicino¹, Amerigo Beneduci², Gianluca Botter³**

6 ¹ Department of Environmental Engineering, University of Calabria, Rende, Cosenza, Italy.

7 ² Department of Chemistry and Chemical Technologies, University of Calabria, Rende, Cosenza,
8 Italy.

9 ³ Department of Civil, Environmental and Architectural Engineering, University of Padua,
10 Padua, Italy.

11 Corresponding author: Alfonso Senatore (alfonso.senatore@unical.it)

12 **Key Points:**

- 13 • More than two-year continuous high-frequency DOC monitoring in two nested sections
14 with different topographic and land cover features
- 15 • Increasing background concentrations during dry summer, but top 10th percentile of
16 discharge associated with up to 79% of total DOC yield
- 17 • Different DOC export processes in the two sections, with hysteretic behaviours non-
18 linearly correlated with the antecedent precipitation

19 **Keywords**

20 Multi-parameter sondes, fDOM, DOC export, DOC hydrological control, hysteresis indices,
21 generalized additive models GAM

22

23 Abstract

24 This study investigates the spatial and temporal dynamics of DOC concentration in a
25 Mediterranean headwater catchment (Turbolo River catchment, southern Italy) equipped with
26 two multi-parameter sondes providing more than two-year (May 2019 to November 2021)
27 continuous high-frequency measurements of several DOC-related parameters. The sondes were
28 installed in two nested sections, a quasi-pristine upstream sub-catchment and a downstream
29 outlet with some anthropogenic disturbances on water quality. DOC estimates were achieved by
30 correcting the fluorescent dissolved organic matter - fDOM - values through an original
31 procedure not requiring extensive laboratory measurements. Then, DOC dynamics at the
32 seasonal and storm event scales were analyzed. At the seasonal scale, results confirmed the
33 climate control on DOC production, with increasing background concentrations in hot and dry
34 summer months. The hydrological regulation proved crucial for DOC mobilization and export,
35 with the top 10th percentile of discharge associated with up to 79% of the total DOC yield. The
36 analysis at the storm scale using flushing and hysteresis indices highlighted substantial
37 differences between the two catchments. In the steeper upstream catchment, the limited
38 capability of preserving hydraulic connection in time with DOC sources determined the
39 prevalence of transport as the limiting factor to DOC export. Downstream, transport- and source-
40 limited processes were observed almost equally. The correlation between the hysteretic
41 behaviour and antecedent precipitation was not linear since the process reverted to transport-
42 limited for high accumulated rainfall values. The study demonstrated the importance of high-
43 resolution measurements to explain DOC dynamics at multiple time scales using a quantitative
44 approach.

45

46 1 Introduction

47 Inland waters receive approximately 70% of the global annual terrestrial net ecosystem
48 production (ca. 5.1 Pg of terrestrial carbon (C) per year; Soares et al., 2019). However,
49 approximately only 1 Pg C is exported from the land to the ocean each year. 65% of exported C
50 is dissolved, with 40% of it being organic (Chaplot and Mutema, 2021). The complex behaviour
51 of dissolved organic carbon (DOC) within inland waters, which can be seen as “active pipelines”
52 contributing to negative net ecosystem production (Cole et al., 2007), needs to be deeply
53 investigated to improve the understanding of the global carbon cycle.

54 Hydrological factors are known to contribute to regulating the DOC balance at the reach
55 scale (Bertuzzo et al., 2017; Parr et al., 2019). Interannual, intra-annual (seasonal) and event-
56 based hydrological variability, particularly in headwater streams (Butman and Raymond, 2011;
57 Rovelli et al., 2018), affects stream-hillslope organic matter exchanges and river network
58 connectivity, leading to significant space and time variations in sources and processes regulating
59 DOC dynamics. The impact of this interaction reflects on broader spatial scales so that, recently,
60 regional approaches have been undertaken to evaluate the relationship between streamflow and
61 DOC export regimes (Morison et al., 2022) or combine streamflow and DOC observations to
62 validate catchment classification (Giesbrecht et al., 2022).

63 At different timescales, different processes emerge. At the seasonal scale, Viza et al.
64 (2022) found that the intermittent flow regime of a Mediterranean river basin contributes to
65 reducing organic matter decomposition rates. More generally, the effects of droughts on DOC

66 transport have being extensively investigated (e.g., Mehring et al., 2013; Humbert et al., 2015;
67 Ahmadi et al., 2019; Wu et al., 2022). Available studies have highlighted the inhibition of DOC
68 release during low flow conditions owing to reduced network connectivity but higher DOC
69 concentrations after droughts.

70 Several studies reported DOC concentration increase in the last decades (e.g., Roulet and
71 Moore, 2006; Monteith et al., 2007; Wu et al., 2022). This trend is connected to rising
72 temperatures that favour the DOC release (Freeman et al., 2001; Bengtson and Bengtsson, 2007;
73 Zhong et al., 2020; Chen et al., 2021), an instance which establishes positive feedback with
74 climate change (since DOC is eventually converted into CO₂, a major greenhouse gas). Other
75 causes, also linked to global warming, can concur to the observed increase of DOC export
76 through the hydrological response, such as changes in land management, pH and sulfate,
77 atmospheric CO₂ increase, acidic deposition decrease and runoff changes (Worrall and Burt,
78 2007).

79 At short timescales of a few days or hours, storm events dominate DOC mobilization and
80 transport (Parr et al., 2019). Precipitation activates direct wet deposition and indirect dry
81 deposition deriving from vegetation canopy and stem (Song et al., 2021) and soil erosion
82 (Chaplot and Mutema, 2021). This contribution to total DOC export is further emphasized if the
83 wet event occurs at the end of prolonged dry periods (Blaurock et al., 2021). Fazekas et al.
84 (2020) highlighted that anomalous events lasting overall less than 20 days in a year could define
85 the annual behaviour of the relationships between streamflow and organic matter concentration.

86 For a specific basin, the concentration-discharge (C-Q) relationship is a signature of the
87 interactions between biogeochemical and hydrological processes, which in their turn depend on
88 climatic, geological and topographical features. C-Q relationships can reveal much of the DOC
89 mobilization dynamics at different timescales (Chorover et al., 2017, Rose et al., 2017). At the
90 seasonal or annual scale, null to low concentration variability in response to discharge
91 fluctuations is called chemostasis (Godsey et al., 2009; Basu et al., 2010), indicating a
92 homogeneous spatial distribution of DOC in the analyzed catchment. On the contrary,
93 chemodynamic behaviour identifies stronger dependence of solute concentration on streamflow
94 (Musolff et al., 2015; Fazekas et al., 2020). This behaviour is characterized by decreasing
95 concentration with discharge if the DOC source is limited or, on the opposite, by increasing
96 concentration with discharge if the limiting factor is the transport capacity. At the event scale,
97 the hysteretic loop's shape and direction help identify the main transport mechanisms. E.g., if the
98 DOC source is close and well-connected to the stream, clockwise hysteretic loops can be
99 identified. On the contrary, counterclockwise loops prevail if it is far and connected by pathways
100 with slow transport velocities.

101 The response of DOC dynamics is strictly connected to spatial features of heterogeneous
102 ecosystems. Several studies showed that not only land cover type and land use (Aitkenhead-
103 Peterson et al., 2007; Vaughan et al., 2017; Fovet et al., 2018; Seybold et al., 2019) but also local
104 topography and geomorphic features (Weiler and McDonnell, 2006) significantly affect DOC
105 mobilization and transport, influencing the hillslope-channel hydraulic connectivity (Botter et al.,
106 2021). Therefore, the response in time of DOC dynamics in specific sections of a catchment is
107 modulated by local properties of the upstream areas. Within the same catchment, significant
108 differences can arise, which cannot be fully captured by a single downstream monitoring section
109 that integrates heterogeneous upstream biogeochemical signals. It is a typical problem of scale
110 (Lowe et al., 2006; McGuire et al., 2014), which also affects streamwater chemistry and needs to

111 be addressed with innovative theoretical concepts and technical approaches, including intensive
112 spatially distributed monitoring campaigns in nested sections of the same catchment (McGuire et
113 al., 2014; Blaurock et al., 2021).

114 DOC dynamics monitoring across different spatial and temporal scales is possible thanks
115 to the advancements in optical aquatic sensors technology. Through in-situ continuous high-
116 frequency measurements, such sensors catch rapidly changing concentrations during storm
117 events and trends over more extended (seasonal to interannual) periods (Pellerin et al., 2014),
118 supporting the development of accurate dynamic models (e.g., Jones et al., 2014) and, in general,
119 providing great potential for a better understanding of aquatic ecosystems functioning (Snyder et
120 al., 2018). Indeed, optical aquatic sensors do not measure DOC directly but rather the fluorescent
121 dissolved organic matter (fDOM), the fraction of DOM that fluoresces. fDOM data can be
122 corrected by accounting for some physical properties of the water (e.g., Watras et al., 2011;
123 Downing et al., 2012; Snyder et al., 2018) and related to DOC using laboratory measurements
124 needed to calibrate the transfer function. Many studies exploit optical sensor properties
125 integrated into multi-parameter sondes to highlight several features of coupled DOC-streamflow
126 dynamics at different timescales. E.g., Saraceno et al. (2009) analyzed a 4-week period including
127 a short-duration storm event. Vaughan et al. (2017) and Fovet et al. (2018) focused on hysteresis
128 in C-Q curves across many storms in catchments with different land use. Mistick and Johnson
129 (2020) analyzed seasonal- and storm-scale DOC responses in clear-cut and forested headwater
130 streams. Blaurock et al. (2021) highlighted the dependency on topography and antecedent
131 wetness conditions. Koenig et al. (2017), Werner et al. (2019), Shogren et al. (2021), and
132 Fazekas et al. (2020) performed multi-year investigations of the C-Q behaviour across multiple
133 sites and timescales.

134 This paper contributes to the ongoing effort to improve understanding of the related
135 dynamics of streamflow and DOC concentration spatial variability across different timescales.
136 Our investigation focused on a Mediterranean headwater catchment (Turbolo River, southern
137 Italy) characterized by dry and hot summer climate enhancing network intermittency. The
138 catchment was equipped with two multi-parameter sondes at two outlets, an upstream section
139 closing a quasi-pristine sub-catchment and a downstream section closing a catchment affected
140 moderately by human activities (agriculture and villages). More than two-year (May 2019 to
141 November 2021) continuous high-frequency measurements of several chemical-physical
142 parameters were recorded, including DOC-related parameters like fDOM, streamwater
143 temperature and turbidity. On-site measurements were complemented by several samples
144 collected during January-April 2021, aimed at characterizing the catchment and calibrating the
145 fDOM-DOC transfer function. Furthermore, hydrometeorological observations, including
146 discharge at the analyzed sections, were continuously performed.

147 The study addresses the interrelated dynamics of DOC concentration, river discharge, and
148 other hydrometeorological variables across multiple timescales in a Mediterranean headwater
149 catchment. This general purpose was fulfilled through two specific objectives, which were
150 addressed by exploiting a novel, simple procedure for the correction of recorded fDOM values
151 that does not rely on extensive laboratory measurements: i) the assessment of the seasonal
152 variability of DOC background values related to several hydrometeorological parameters in two
153 nested sections characterized by different land uses; ii) the evaluation of the DOC concentration-
154 discharge relationships at the storm event timescale, considering season- and site-dependence,
155 aimed at uncovering the main mobilization and transport mechanisms. For both the timescales

156 considered in this study (storm event and seasonal), the difference in DOC response of the two
157 nested cross-sections was analyzed to infer the dependence of DOC dynamics on scale properties
158 and other landscape features.

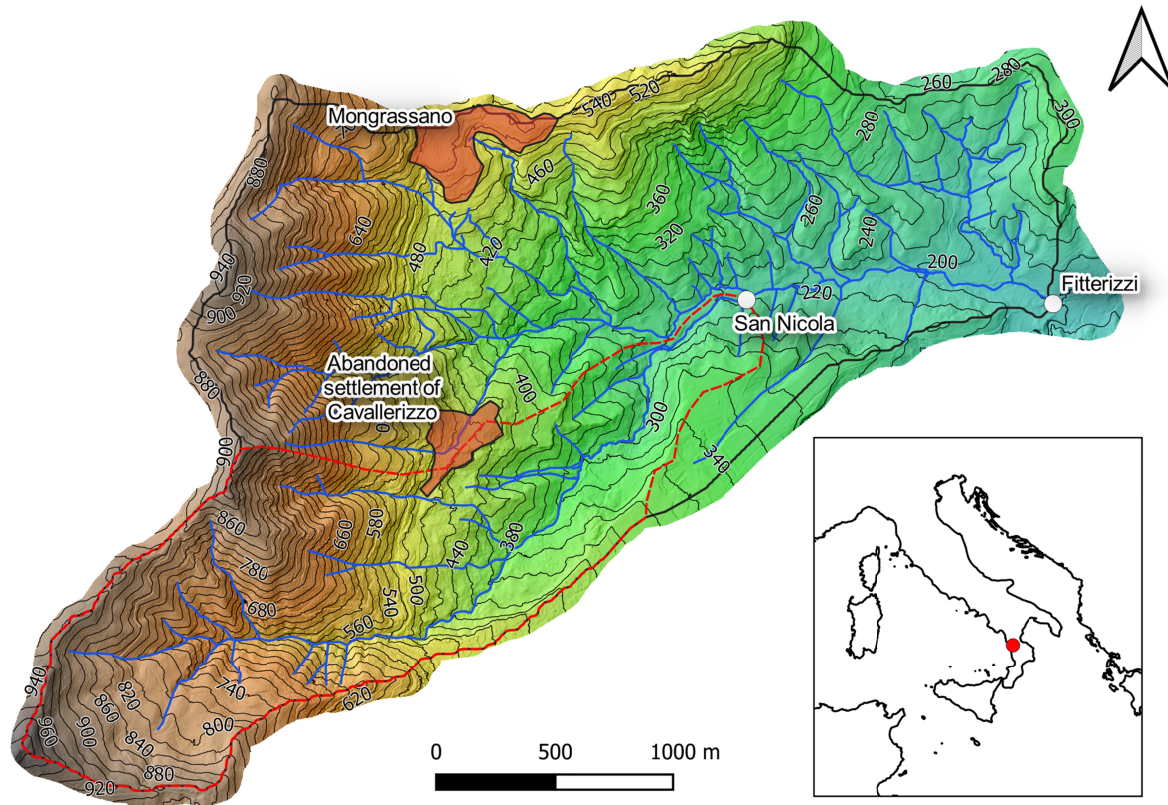
159

160 **2 Data and Methods**

161 2.1 Study area

162 The study area is the upper Turbolo creek catchment (Figure 1), closed at the Fitterizzi
163 gauge (183 m a.s.l.), in southern Italy, a drought-prone area (Mendicino and Versace, 2007), for
164 which an increasing drying scenario is projected (Senatore et al., 2022a). The catchment area is
165 approximately 7 km², with an elevation of up to 1005 m a.s.l. The Turbolo creek originates from
166 the Calabrian Coastal Range, which is dominated by strongly altered and fractured crystalline-
167 metamorphic rocks that entail widespread slope instability and have overall high permeability.
168 The geology allows ample groundwater recharge and storage that sustains almost perennial flow
169 at the Fitterizzi gauge. Steep slopes characterize the catchment on the metamorphic rocks in the
170 west. In the eastern part, slopes are less steep but affected by water erosion processes, inducing
171 shallow landslides and soil creep (Senatore et al., 2020).

172 The channel network consists of two main forks: the southern one (red-contoured on the
173 map) is the San Nicola creek, 2 km² wide, in whose closing section (231 m a.s.l.) a gauging
174 station was installed. San Nicola is a quasi-pristine sub-catchment on which only an abandoned
175 settlement is located. The average elevation of the catchment closed at the San Nicola gauge is
176 600 m a.s.l. The northern fork reflects some more relevant anthropogenic effects, with more
177 agricultural areas (mainly non-irrigated arable land and olive groves) and the village of
178 Mongrassano with an adjoining sewage treatment plant sized for about 500 equivalent
179 inhabitants. The average elevation of the catchment (closed at the Fitterizzi gauge) is 491 m a.s.l.



180

181 **Figure 1.** The Turbolo catchment closed at the Fitterizzi outlet. The sub-catchment closed at the
 182 San Nicola gauge is contoured by a dashed red line.

183 2.2 Continuous-time monitoring and manual sampling of water quality

184 Several chemical-physical parameters were recorded continuously with an hourly time
 185 step starting from May 2019 by two multiparametric probes located in the San Nicola (SN) and
 186 Fitterizzi (FIT) sites. Monitoring is ongoing, but the results presented here relate to observations
 187 performed until 25 November 2021. Two YSI EXO2™ multi-parameter water quality sondes
 188 with 7 sensor ports, including a central wiper port, were used. Among the many parameters
 189 monitored (namely, ammonia NH_3 , specific conductance SpCond, Fluorescent Dissolved
 190 Organic Matter fDOM, nitrate ions NO_3^- -N, dissolved oxygen DO, ammonium ions NH_4^+ -N,
 191 redox potential ORP, salinity Sal, total dissolved solids TDS, pH, temperature T and turbidity),
 192 Table 1 shows the availability in time for both SN and FIT of fDOM, T and turbidity, needed for
 193 DOC calculation.

194 Continuous observations were supported by discrete monitoring carried out in January-
 195 April 2021, when 59 samples were collected on-field and analyzed in the laboratory according to
 196 Italian (APAT-IRSA) standards to achieve reference DOC values, used for the correction of
 197 measured fDOM values. Besides DOC measurements, several other physico-chemical
 198 parameters were measured to characterize the catchment in a larger picture and validate further
 199 continuous observations.

200 Finally, meteo-hydrological observations carried out at both sites were available for the
 201 whole period. Specifically, a weather station and a water stage gauge were installed in FIT,

202 managed by the Regional Agency for the Protection of the Environment (ARPACal), while a
 203 water stage gauge operated in SN until March 2021.

204

205 **Table 1.** Data sampling timesheet.

206

FIT			SN		
Start date	End date	Hourly samples	Start date	End date	Hourly samples
22/05/2019 18:00	19/11/2019 11:00	4338	22/08/2019 18:00	16/12/2019 12:00	2779
16/01/2021 13:00	06/10/2021 06:00	6306	05/01/2020 11:00	30/01/2020 10:00	600
18/10/2021 14:00	26/11/2021 00:00	923	05/04/2020 10:00	25/11/2020 10:00	5617
			01/12/2020 11:00	25/03/2021 10:00	2736
Total 11567			Total 11732		

207

208 2.3 Correction of measured fDOM values

209 In the aim of acquiring DOC timeseries starting from fDOM measurements, the first
 210 correction was applied to the raw data to account for the fDOM signal decrease as a function of
 211 temperature implied by the increase of non-radiative deactivation pathways (Watras et al., 2011):

212

$$213 \quad fDOM_T = fDOM / [1 + \rho(T_m - T_r)] \quad (1)$$

214

215 In the above equation, T_m and T_r are measured and reference temperatures in °C, and ρ is
 216 a specific temperature attenuation coefficient (°C⁻¹) equal to -0.01°C⁻¹ (Exo User Manual, 2020).

217 Then, a suspended particle attenuation factor k was estimated to correct the values of
 218 $fDOM_T$ using the following equation (Downing et al., 2012):

219

$$220 \quad fDOM_{corr} = \frac{fDOM_T}{e^{k \cdot turb}} \quad (2)$$

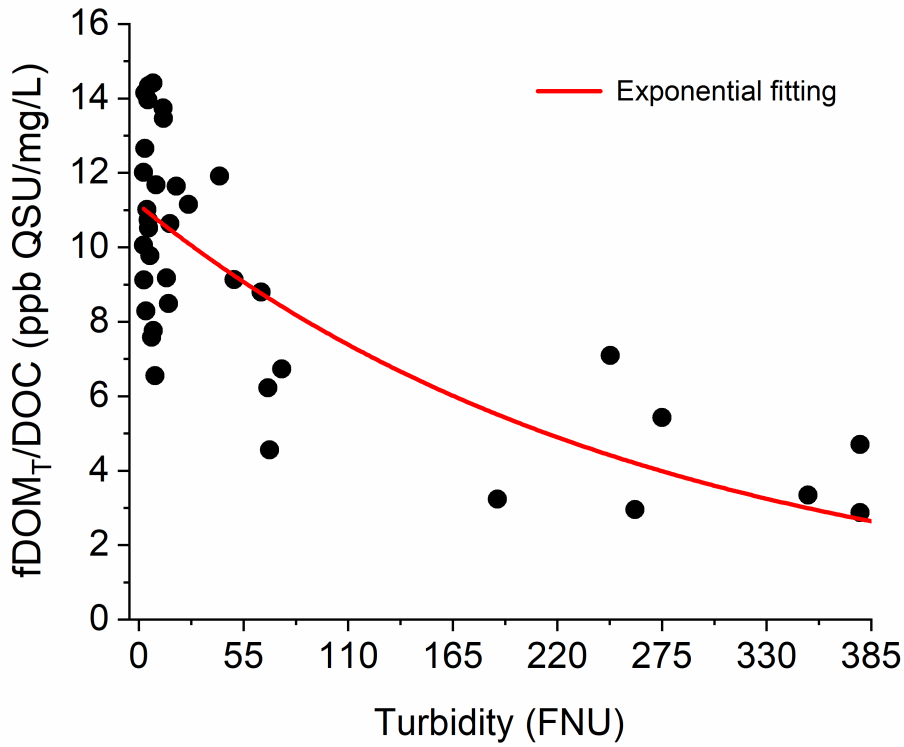
221

222 where $turb$ is the turbidity.

223 The factor $k = 0.004 \pm 0.001$ FNU⁻¹ was calibrated using water samples collected under
 224 various conditions and analyzed in the laboratory (Figure 2).

225

226



227

228 **Figure 2.** Dispersion plot of the parameter $fDOM_T/DOC$ as a function of the turbidity.

229

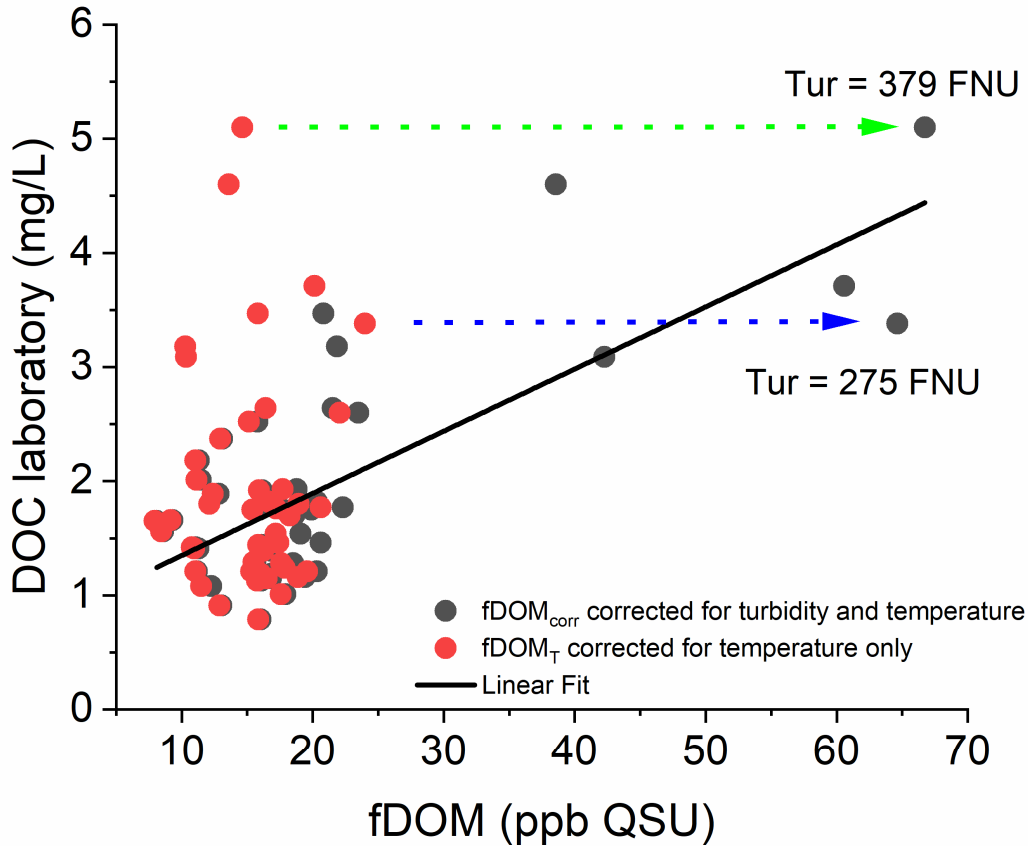
230 Finally, assuming a linear relationship between $fDOM_{corr}$ and DOC:

231

$$232 \quad DOC = m \cdot fDOM_{corr} + c \quad (3)$$

233

234 The concentration of DOC was estimated. The parameters at eq. (3) were calibrated
 235 through linear fitting (using $c = 0.8 \pm 0.2$ and $m = 0.054 \pm 0.007$, Figure 3).



236

237 **Figure 3.** Correlation analysis between the laboratory DOC values measured on discrete samples
 238 and the corresponding fDOM_{corr} values (grey circles). The corresponding fDOM_T values are also
 239 reported (red circles).

240

241 For turbidity values much higher than those used to estimate the factor k , equation (2)
 242 could not be applied. Therefore, for continuous measurements with turbidity values higher than
 243 600 FNU, DOC values were extrapolated using multiple linear regressions of discharge and
 244 accumulated precipitation from 1 up to 12 previous hours. Such regressions reached R^2 values up
 245 to 0.7 compared to observations.

246

247 **2.4 Event Selection and Indices Calculation**

248 A set of 29 focus events for each sub-catchment were identified during the study period
 249 following the approach proposed by Landson et al. (2013). At first, the baseflow was separated
 250 from quickflow using the following basic filter equations:

251

$$q_f(i) = \begin{cases} \alpha q_f(i-1) + \frac{(1-\alpha)}{2} [q(i) - q(i-1)] & \text{for } q_f(i) > 0 \\ 0 & \text{otherwise} \end{cases} \quad (4)$$

$$q_b(i) = q(i) - q_f(i) \quad (5)$$

254

255 Where $q_f(i)$, $q(i)$, and $q_b(i)$ are the quickflow, the streamflow, and the baseflow
 256 response at the i^{th} sampling time (hourly), and α the filter parameter. This iterative method must
 257 be run multiple times (called *passes*) forward and backward. Thereafter, the Baseflow Index
 258 (BFI), defined as the ratio between the baseflow and the streamflow volume, was used to identify
 259 the events. The events selection based on this method was performed through the “hydroEvents”
 260 package in Software R using $\alpha = 0.925$, while the appropriate number of passes to separate the
 261 baseflow for hourly data was chosen equal to 9, as suggested by Landson et al. (2013). The
 262 method adopted not always detected events in both catchments during the same storm.
 263 Furthermore, some minor events, though automatically detected, were discarded due to the very
 264 low flow associated, especially in the small San Nicola creek.

265 The hysteresis index HI and the flushing index FI were calculated to evaluate the
 266 dynamics of DOC concentration in the analyzed basin, which is mobilized and transported by
 267 storm events.

268 The hysteresis index HI indicates a clockwise or counterclockwise behaviour in the
 269 concentration-discharge (C-Q) relationship (Lloyd et al., 2016, Vaughan et al., 2017). For each
 270 event, the HI index was calculated starting from the normalized values of discharges and DOC
 271 concentrations:

272

$$Q_{i,norm} = \frac{Q_i - Q_{min}}{Q_{max} - Q_{min}} \quad (6)$$

$$C_{i,norm} = \frac{C_i - C_{min}}{C_{max} - C_{min}} \quad (7)$$

275

276 where Q_i and C_i are the discharge and the DOC concentration at the i^{th} time step, Q_{min}
 277 and Q_{max} are the maximum and minimum discharge values, respectively, and C_{min} and C_{max} are
 278 the maximum and minimum DOC concentrations of the storm event. These normalized
 279 concentrations $C_{i,norm}$ were interpolated by linear regression using two adjacent measurements
 280 with an interval of 2%. For the same intervals (called j), the hysteresis index HI_j was calculated
 281 as follows:

282

$$HI_j = C_{j,rising} - C_{j,falling} \quad (8)$$

284

285 where $C_{j,rising}$ and $C_{j,falling}$ are the DOC concentrations in the rising and falling limb,
 286 respectively. The final hysteresis HI (ranging from -1 to +1) of each storm event was obtained by
 287 averaging all HI_j values. Positive HI values indicate a clockwise hysteresis, while negative
 288 values indicate a counterclockwise hysteresis.

289 The flushing index (FI) evaluates the increase of concentration, i.e., flushing effect
 290 (positive values), or the decrease of concentration, i.e., diluting (negative values) effect of DOC
 291 concentration on the rising limb (Butturini et al. 2008, Vaughan et al. 2017). The FI index is
 292 defined as:

$$293$$

$$294 \quad FI = C_{Qpeak,norm} - C_{initial,norm} \quad (9)$$

295

296 where $C_{Qpeak,norm}$ and $C_{initial,norm}$ are the normalized DOC concentrations at the peak
 297 of discharge and the beginning of the storm, respectively.

298

299 **3 Results**

300 **3.1 Seasonal variability of background DOC concentration**

301 The mean concentration of dissolved organic carbon across the monitoring campaign
 302 (2019-2021) for FIT and SN were $1.7 \pm 0.3 \text{ mg l}^{-1}$ and $2.1 \pm 0.5 \text{ mg l}^{-1}$, respectively. These are
 303 relatively low values in agreement with typical DOC concentrations in freshwater ($\leq 5 \text{ mg l}^{-1}$)
 304 (Stumm and Morgan, 1996). Concentrations between the two sites might not be directly
 305 comparable because the two recording periods do not entirely overlap. However, reducing the
 306 statistics only to the 91 non-rainy days with overlapping observations, DOC concentrations were
 307 higher in the SN section ($1.8 \pm 0.3 \text{ mg l}^{-1}$ and $1.9 \pm 0.4 \text{ mg l}^{-1}$ for FIT and SN, respectively).
 308 Slightly higher background values for the upstream monitoring section can be due to the
 309 enhanced biomass production and decomposition and the steeper topography of the upstream
 310 forested catchment.

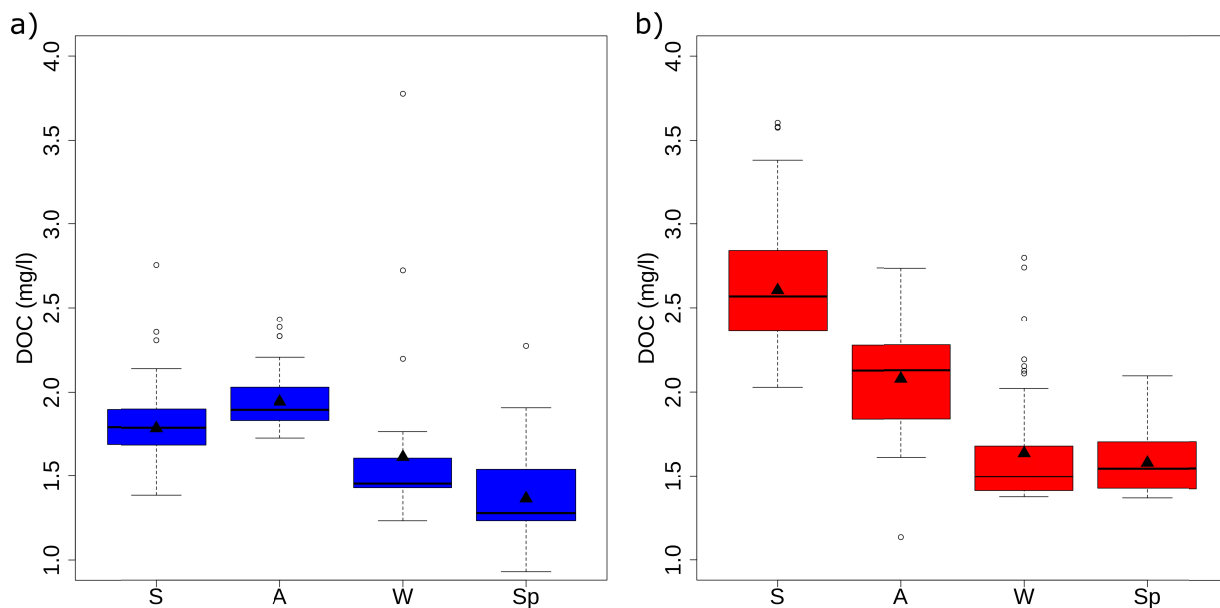
311 Table 2 reports the descriptive statistics on the background values (days in the absence of
 312 rain) of FIT and SN sites for the entire monitoring campaign. Box and whisker plots of the DOC
 313 showing seasonal trends are given in Figure 4 for both locations. The analysis was conducted on
 314 average daily values, and the set of data corresponding to each site was also divided into four
 315 categories corresponding to calendar seasons - spring (Sp), summer (S), autumn (A) and winter
 316 (W). The two sites showed partially contrasting behaviour. For FIT, the downstream site, the
 317 highest average DOC was recorded in autumn, with a descending order of $A > S > W > Sp$. In SN,
 318 the upstream site, the descending order was similar. Still, the highest average DOC was observed
 319 in summer ($S > A > W > Sp$) instead of autumn, probably due to the greater availability of organic
 320 material in the surrounding pristine area that during the summer is converted into DOC by
 321 photochemical processes. Furthermore, lower autumn temperatures in SN than in FIT due to the
 322 higher mean altitude of the contributing catchment inhibit DOC production and export. The
 323 analysis suggested that the difference between mean and median values is larger in winter for
 324 both sites. This result is connected to the more frequent high-discharge events observed in
 325 winter, whose effects can be seen on the non-rainy days considered in this analysis. The one-way
 326 ANOVA statistical analysis showed that the four data sets associated with each season were
 327 significantly different (FIT $p > 2.97 \times 10^{-43}$; SN $p > 1.70 \times 10^{-71}$).

328 **Table 2.** Descriptive statistics on the data set of seasonal background DOC values (Sp: spring; S:
 329 summer; A: autumn; W: winter).

330

	DOC Fitterizzi (mg l^{-1})				DOC San Nicola (mg l^{-1})			
	Sp	S	A	W	Sp	S	A	W
Min	0.93	1.38	1.73	1.23	1.37	2.03	1.13	1.37
Max	2.27	2.76	2.43	3.78	2.09	3.61	2.74	2.8
Mean	1.36	1.78	1.94	1.61	1.58	2.61	2.08	1.64
SD	0.22	0.19	0.17	0.47	0.17	0.34	0.26	0.36
Median	1.28	1.79	1.89	1.45	1.54	2.57	2.13	1.50
N° obs	92	162	58	33	64	102	78	47

331



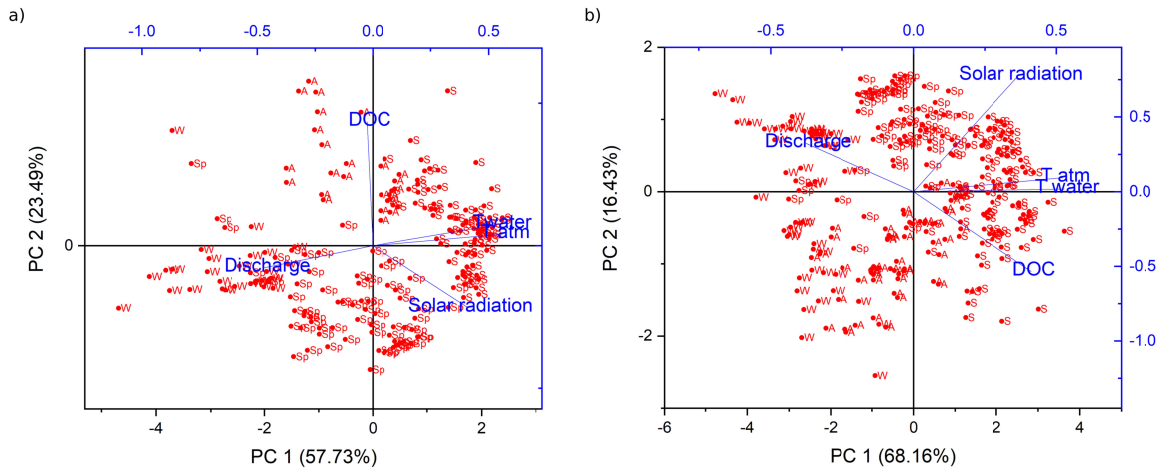
332

333 **Figure 4.** Box and whisker plots of temporal variation of background seasonal DOC values at
 334 Fitterizzi and San Nicola stations. Black triangles represent seasonal means.

335

336 To find potential correlations between DOC and key hydrometeorological parameters
 337 recorded in FIT, the data were further processed by multivariate data statistical analysis. Figure 5
 338 shows the principal component analysis, including DOC and water temperature, air temperature,
 339 solar radiation, and discharge. For both sites, PC1 and PC2 altogether explained more than 80%
 340 of the total variance, and seasonal clusters could be distinguished with a clear temporal
 341 trajectory. Both PCA plots confirm the univariate statistical analysis presented before, indicating
 342 higher DOC concentrations were found mainly in summer and, in addition, provide us with
 343 further interesting insights because the DOC was negatively affected by the discharge. Indeed,
 344 the DOC decreased in a counterclockwise direction from summer to spring. The other
 345 meteorological parameters examined positively correlate to DOC since they determined the
 346 weather conditions in summer and spring. The DOC was higher in summer due to the
 347 concentration effect that the catchment undergoes during this season. However, solar radiation

348 and temperature may strongly affect the quantity and quality of the DOC through the
 349 enhancement of several photocatalytic degradation processes of dissolved organic matter
 350 (Stumm and Morgan, 1996).
 351

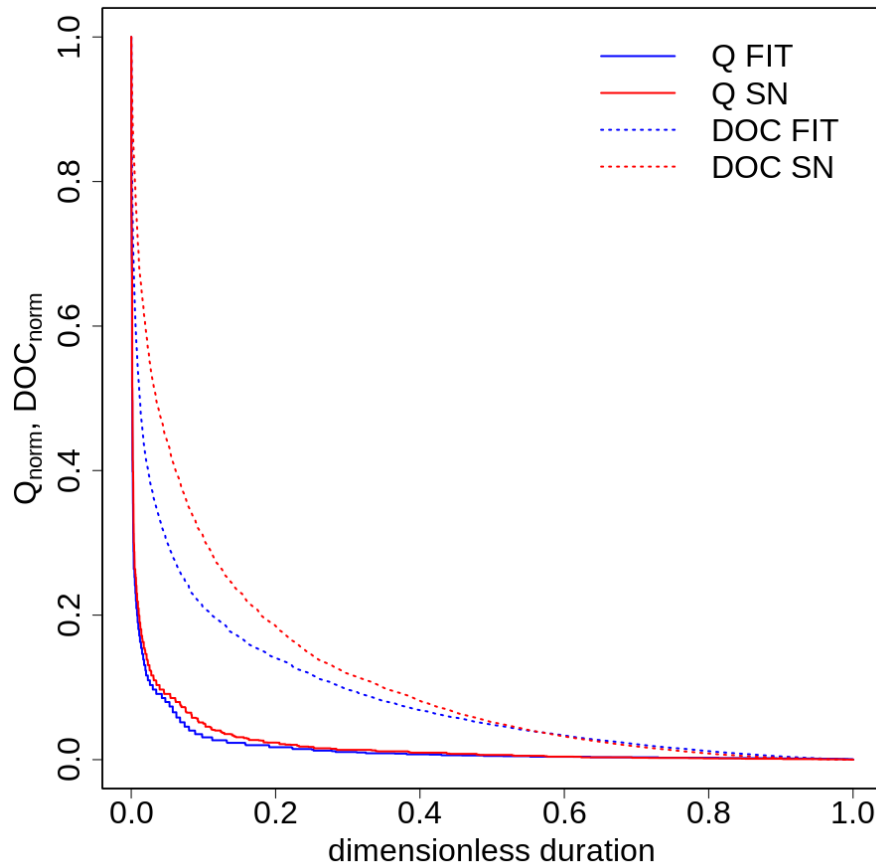


352
 353 **Figure 5.** Principal component analysis for background seasonal data sets collected in a)
 354 Fitterizzi and b) San Nicola.

355

356 3.2 Hydrological controls on DOC export

357 Most of the export through streamflow occurred relatively quickly, i.e. during high flow
 358 events. Discharges above Q10 (i.e., the flow equalled or exceeded only 10% of the time) were
 359 responsible for 79% of the total yield in FIT (which is equal to $15.3 \cdot 10^3$ kg in 11567 hours) and
 360 69% in SN ($4.4 \cdot 10^3$ kg in 11732 hours). Figure 6 shows the steep slopes of the flow duration
 361 curves in both sites, emphasising the high flow variability and the significant impact of
 362 quickflow. Corresponding normalized accumulated DOC load curves are also quite convex. The
 363 lower convexity of the SN DOC load curve highlights the relatively more consistent DOC
 364 contribution in this more forested catchment with moderate to high discharges.



365

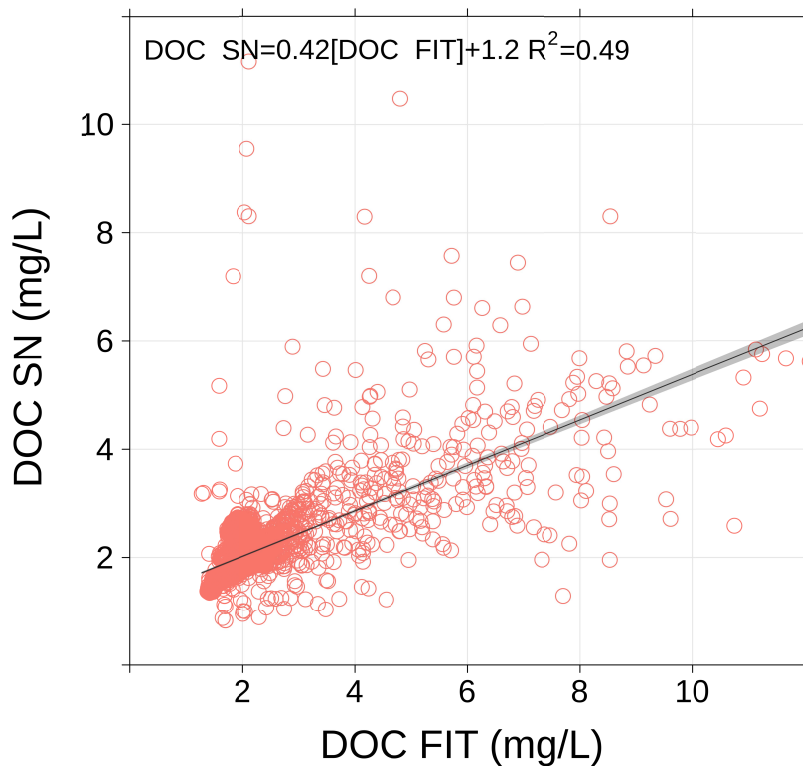
366 **Figure 6.** Flow duration curves and corresponding normalized accumulated DOC loads for SN
 367 and FIT. It is noteworthy that, while flow duration curves are increasing by definition,
 368 corresponding load curves are not because DOC load could be higher with lower discharge
 369 values. Nevertheless, this behaviour, which can be detected especially in the low flow tail, is of
 370 little significance in this case.

371

372 The behaviour of DOC concentrations in FIT and SN were evaluated by comparing 3760
 373 data (hourly time step) acquired simultaneously at both sections during August-November 2019
 374 and January-March 2021. Figure 7 shows that DOC concentration was generally higher in FIT
 375 (61% of the time) than in SN. This result, which overturns the indications obtained in the
 376 previous seasonal analysis, highlights the importance of the rain/discharge events determining
 377 the highest concentration values. The total yield measured in the overlapping measurements
 378 period was equal to $12.5 \cdot 10^3$ kg and $2.3 \cdot 10^3$ kg, respectively, for FIT and SN, leading to a ratio
 379 between the two total yields of 5.4, which is higher than the ratio between the two catchment
 380 areas, approximately equal to 3.5.

381 The FIT catchment is characterized, overall, by a flatter topography. It is influenced by
 382 the significant contribution of the upstream northern fork, having different (less forested, more
 383 agricultural) land use and more relevant water erosion processes. It is plausible that DOC
 384 sources' connection to the active drainage network in FIT is more dependent on rain events. On
 385 the other hand, the SN discharge regime, mainly controlled by groundwater sources with lower

386 DOC concentration (mountain springs), can reduce the effect of DOC sources' contribution
 387 activated by rain events. Indeed, for the overlapping period, DOC concentrations were more
 388 positively correlated to the discharge observed in FIT than SN (correlation coefficient r equal to
 389 0.65 and 0.34, respectively). This result is consistent with the behaviour of the accumulated DOC
 390 load curves in Figure 6, confirming the more substantial impact of high flows in FIT on DOC
 391 yield.



392

393 **Figure 7.** Comparison between simultaneous FIT and SN DOC observations.

394

395 The importance of storms and consequent high flows in the regulation of DOC export
 396 stands at the basis of the event-based analysis shown in the following. 29 events were selected
 397 for each station, 19 representing the response produced in the two sections by the same storm.

398 Tables 3 and 4 provide some statistics on the selected events. Mean and maximum
 399 discharge values were higher in FIT (average values of $0.627 \text{ m}^3 \text{ s}^{-1}$ and $1.517 \text{ m}^3 \text{ s}^{-1}$, respectively)
 400 than in SN (average values of $0.208 \text{ m}^3 \text{ s}^{-1}$ and $0.487 \text{ m}^3 \text{ s}^{-1}$, respectively). Consistently with
 401 results shown in Figure 7, mean and maximum DOC concentrations were higher in FIT (average
 402 values of 4.03 mg l^{-1} and 8.45 mg l^{-1} , respectively) than in SN (average values of 3.31 mg l^{-1} and
 403 6.78 mg l^{-1} , respectively).

404 **Table 3.** Storms statistics for FIT. Dates marked with * are also considered in SN.

Start date/time	End date/time	Time (h)	Mean discharge ($\text{m}^3 \text{s}^{-1}$)	Max discharge ($\text{m}^3 \text{s}^{-1}$)	Mean DOC (mg l^{-1})	Max DOC (mg l^{-1})	HI	FI
28/05/2019 06:00	29/05/2019 00:00	18	0.103	0.179	2.38	5.61	-0.27	0.17
15/07/2019 20:00	16/07/2019 15:00	19	0.097	0.309	7.05	19.88	-0.26	0.28
23/09/2019 22:00	24/09/2019 15:00	17	0.027	0.057	3.14	6.17	-0.51	0.10
07/10/2019 02:00*	08/10/2019 07:00	29	0.065	0.217	4.43	8.83	0.17	1.00
03/11/2019 21:00*	04/11/2019 17:00	20	0.080	0.217	5.03	9.78	0.03	0.73
05/11/2019 14:00*	07/11/2019 17:00	51	0.049	0.260	2.60	5.76	-0.05	0.38
11/11/2019 16:00	12/11/2019 16:00	24	0.083	0.146	4.16	7.32	0.04	0.65
13/11/2019 00:00*	14/11/2019 03:00	27	0.121	0.362	4.35	8.53	0.00	0.90
17/01/2021 13:00*	18/01/2021 17:00	28	0.370	1.226	3.50	8.54	0.27	0.99
23/01/2021 04:00*	23/01/2021 19:00	15	0.508	1.956	4.42	10.75	0.10	0.41
23/01/2021 18:00*	24/01/2021 05:00	11	0.506	1.165	4.14	10.75	0.31	0.00
24/01/2021 03:00*	25/01/2021 14:00	35	2.182	6.796	7.38	17.72	-0.03	0.52
25/01/2021 17:00*	26/01/2021 13:00	20	2.471	5.200	6.40	12.08	-0.02	0.59
31/01/2021 14:00*	01/02/2021 14:00	24	1.224	2.407	4.31	7.57	-0.09	0.04
31/01/2021 22:00*	01/02/2021 14:00	16	1.404	2.407	4.92	7.57	0.00	0.36
01/02/2021 21:00*	02/02/2021 12:00	15	1.536	2.812	4.53	8.02	0.11	0.04
08/02/2021 00:00*	09/02/2021 00:00	24	0.684	1.564	2.48	6.15	0.26	0.57
09/02/2021 00:00*	10/02/2021 00:00	24	0.734	1.290	3.01	5.06	-0.02	0.79
10/02/2021 13:00*	11/02/2021 13:00	24	1.644	4.721	5.31	12.99	0.20	0.54
13/02/2021 09:00*	14/02/2021 02:00	17	1.352	2.707	3.91	6.33	0.27	0.92
14/03/2021 16:00*	15/03/2021 15:00	23	0.225	0.542	2.47	6.11	-0.11	0.88
19/03/2021 19:00*	20/03/2021 19:00	24	0.598	1.564	3.84	7.05	0.33	0.84
20/03/2021 16:00*	22/03/2021 05:00	37	1.071	2.219	4.49	9.13	0.18	0.17
23/04/2021 12:00	24/04/2021 23:00	35	0.524	1.226	3.22	5.85	0.23	0.68
17/07/2021 13:00	19/07/2021 17:00	52	0.034	0.396	2.31	6.14	-0.36	0.70
26/08/2021 15:00	27/08/2021 02:00	11	0.028	0.060	3.30	6.87	-0.15	0.32
11/09/2021 06:00	11/09/2021 22:00	16	0.060	0.182	2.81	3.35	-0.38	0.78
25/10/2021 14:00	26/10/2021 09:00	19	0.088	0.158	2.65	4.28	-0.14	0.87
01/11/2021 17:00	02/11/2021 15:00	22	0.308	1.638	4.46	10.73	0.07	0.77

406 **Table 4.** Storms statistics for SN. Dates marked with * are also considered in FIT.

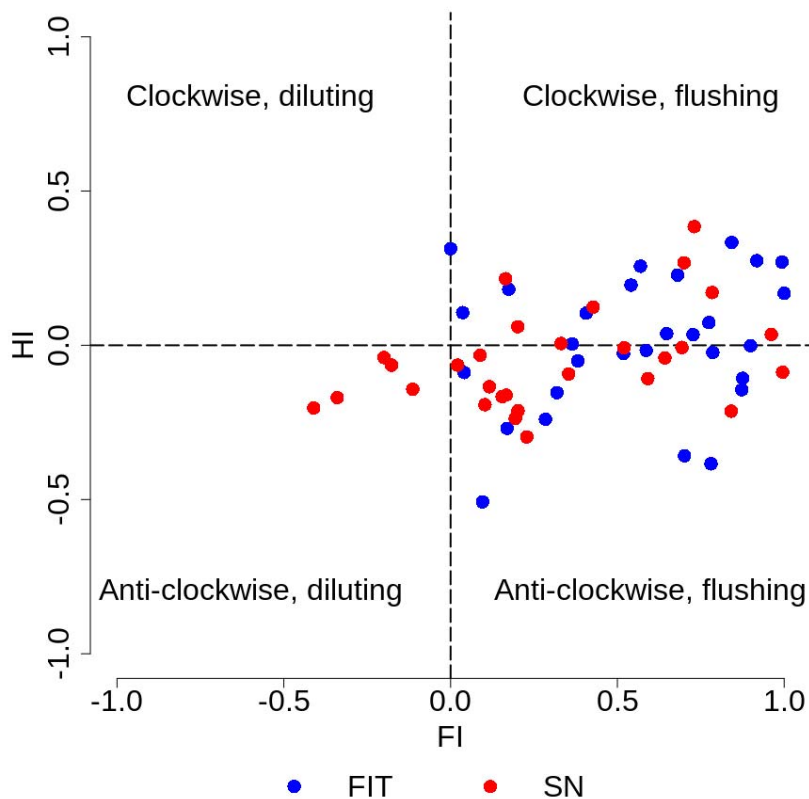
Start date/time	End date/time	Time (h)	Mean discharge ($\text{m}^3 \text{s}^{-1}$)	Max discharge ($\text{m}^3 \text{s}^{-1}$)	Mean DOC (mg l^{-1})	Max DOC (mg l^{-1})	HI	FI
07/10/2019 12:00*	08/10/2019 02:00	14	0.019	0.044	3.23	7.58	0.01	0.33
03/11/2019 14:00*	04/11/2019 18:00	28	0.013	0.069	3.40	8.36	0.06	0.20
05/11/2019 14:00*	07/11/2019 17:00	51	0.009	0.056	2.18	5.49	-0.30	0.23
12/11/2019 22:00*	14/11/2019 01:00	27	0.027	0.077	2.81	7.31	-0.21	0.20
09/12/2019 08:00	10/12/2019 13:00	29	0.112	0.311	1.57	2.14	-0.01	0.52
04/07/2020 12:00	05/07/2020 09:00	21	0.018	0.050	2.91	5.40	-0.11	0.59
08/08/2020 08:00	09/08/2020 07:00	23	0.010	0.025	3.30	4.58	0.17	0.78
25/09/2020 15:00	26/09/2020 20:00	29	0.028	0.140	3.87	7.00	0.04	0.96
28/09/2020 08:00	29/09/2020 07:00	23	0.084	0.480	4.26	11.26	-0.01	0.69
15/10/2020 06:00	16/10/2020 04:00	22	0.035	0.077	3.02	5.36	0.38	0.73
08/12/2020 21:00	10/12/2020 01:00	28	0.399	0.959	2.65	4.36	-0.17	-0.34
30/12/2020 21:00	31/12/2020 10:00	13	0.339	0.517	5.32	10.99	-0.06	-0.18
09/01/2021 13:00	10/01/2021 13:00	24	0.136	0.430	4.54	9.52	-0.19	0.10
15/01/2021 06:00	16/01/2021 09:00	27	0.156	0.304	4.07	7.61	-0.16	0.17
17/01/2021 13:00*	18/01/2021 17:00	28	0.102	0.337	3.41	8.30	-0.16	0.12
23/01/2021 04:00*	23/01/2021 19:00	15	0.158	0.537	3.46	6.80	-0.09	0.35
23/01/2021 18:00*	24/01/2021 05:00	11	0.136	0.320	3.48	7.20	-0.04	-0.20
24/01/2021 02:00*	25/01/2021 08:00	30	0.641	1.867	4.56	9.13	-0.20	-0.41
25/01/2021 17:00*	26/01/2021 13:00	20	0.680	1.428	3.38	5.62	-0.24	0.19
31/01/2021 14:00*	01/02/2021 14:00	24	0.338	0.661	2.90	4.78	-0.14	-0.11
31/01/2021 22:00*	01/02/2021 14:00	16	0.390	0.661	3.08	4.78	-0.06	0.02
01/02/2021 21:00*	02/02/2021 12:00	15	0.421	0.773	3.22	4.57	-0.03	0.09
08/02/2021 00:00*	09/02/2021 00:00	24	0.190	0.430	2.21	5.89	-0.09	1.00
09/02/2021 00:00*	10/02/2021 00:00	24	0.203	0.354	2.49	6.24	-0.17	0.15
10/02/2021 13:00*	11/02/2021 12:00	23	0.463	1.297	3.27	5.26	-0.04	0.64
13/02/2021 09:00*	14/02/2021 02:00	17	0.371	0.744	3.41	10.48	0.22	0.16
14/03/2021 16:00*	15/03/2021 15:00	23	0.062	0.149	2.33	5.71	-0.21	0.84
19/03/2021 18:00*	20/03/2021 17:00	23	0.166	0.430	3.31	6.61	0.12	0.43
20/03/2021 16:00*	21/03/2021 21:00	29	0.328	0.610	4.27	8.42	0.27	0.70

407

408 Analyzing the indices accounting for DOC concentration during storms helps understand
409 the nature of the relevant mobilization and export processes driving DOC dynamics in stream
410 water. Figure 8 provides a comprehensive overview of the catchment response during these
411 events by comparing the two sites' hysteresis (HI) and flushing (FI) indices. In FIT and SN,
412 positive FI values largely prevailed (only SN showed 5 out of 29 slightly negative values). A
413 positive flushing index means that the DOC sources in the regions that contribute to the fast
414 response of the catchment (root zone and riparian areas) are abundant enough to increase
415 concentration when discharge increases (rising limb of the hydrograph).

416 HI results provided more contrasting information. In FIT, HI values were equally
417 subdivided into positive and negative, with few values practically equal to zero. In SN, 8 values
418 out of 29 were positive, but the general behaviour was not very different from FIT. HI values for
419 the two sections during the 19 simultaneous events were correlated quite well ($r = 0.63$).
420 Negative HI values represent counterclockwise behaviour in the concentration–discharge (C-Q)

421 graphs, meaning that DOC concentration is higher in the falling limb of the hydrograph than in
 422 the rising. This behaviour generally occurs when the primary DOC sources are relatively far and
 423 hydraulically disconnected from the active river network at the beginning of the storm or when
 424 DOC transport is lower than water flux into the channel. Negative values of HI might also imply
 425 that the export process is transport-limited, i.e., the process ceases because of the reduced
 426 transport capacity when the water drains towards the watercourse. On the other hand, positive HI
 427 values mean clockwise behaviour in the C-Q graphs, higher concentrations in the rising limb, the
 428 proximity of the major DOC sources to the active network, and source-limited process, i.e.,
 429 despite a still sustained water flow from the catchment to the river network, DOC concentration
 430 reduces in time. Therefore, the HI index allows quantifying event hysteresis dynamics, even with
 431 complex patterns (Williams, 1989) that are not easily interpretable. Overall, the slightly higher
 432 number of negative HI values in SN can be correlated to lower hydraulic connectivity of the
 433 upstream mountainous, steep catchment, presenting more accentuated flow spatial intermittency
 434 than FIT, as is typical for the headwater catchments.



435

436 **Figure 8.** Storm hysteresis index (HI) versus storm flushing index (FI) for FIT and SN.

437

438 Beyond the observed differences between the upstream and downstream sections, no
 439 general rules exhaustively explained the occurrence of clockwise/counterclockwise hysteresis
 440 during flow events. In SN, positive HI values were observed at the end of the winter, consistently
 441 with enhanced hillslope-channel hydraulic connectivity at the end of the wet season. Three
 442 positive HI events were detected from 13.02.2021 to 21.03.2021 (Table 4), also providing the

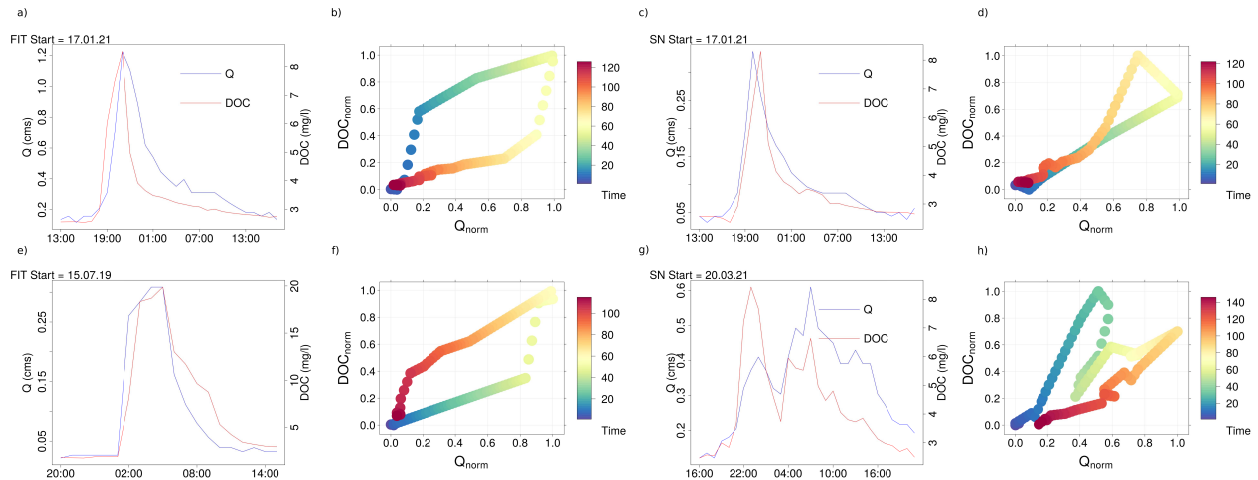
443 highest loads due to the corresponding high discharges. Nevertheless, four events with $HI > 0$
444 occurred in early autumn (07.10.2019, 03.11.2019, 25.09.2020 and 15.10.2020) and one even in
445 summer (08.08.2020). However, all these events were characterized by very low flows (the
446 maximum peak flow overcame $0.1 \text{ m}^3 \text{ s}^{-1}$ only in one case), therefore providing a relatively low
447 contribution in terms of DOC load. The maximum discharges of the events were weakly
448 negatively correlated to HI values ($r = -0.21$), while correlations with FI were stronger ($r = -$
449 0.43). The latter result can be explained by considering that DOC removal might become supply-
450 limited during high-intensity events. Indeed, the average maximum discharge of the 5 diluting
451 events in SN was almost double ($0.865 \text{ m}^3 \text{ s}^{-1}$) that of all events.

452 The positive HI values in FIT events occurred only in autumn and winter (Table 3). The
453 only exception was given by one positive HI event in spring (23.04.2021), which, however, took
454 place immediately after the wet winter season. Furthermore, the most negative index values
455 occurred all in late spring/summer, with generally dry conditions. HI values were positively
456 correlated with the maximum discharges of the events ($r = +0.32$), while FI correlations were
457 weaker than SN ($r = -0.12$).

458 Figure 9 shows examples of hydrographs, DOC chemographs and the corresponding C-Q
459 relations for FIT and SN in the case of positive and negative HI values. Specifically, the
460 17.01.2021 event (Figs. 9a-d) concerned both catchments, with opposite HI signs (-0.16 and
461 $+0.27$, in SN and FIT, respectively). This event is peculiar because the DOC concentration
462 evolution had similar behaviour and was synchronous in the two sections, occurring at the same
463 time as the FIT discharge peak, while the discharge peak in SN was brought forward by one
464 hour. In SN, despite the flow reduction, DOC concentration increased for the hour following the
465 peak flow, contrasting the decrease in the total load. This result can be interpreted considering
466 that the time needed to reach the peak flow in FIT corresponded to the time required to mobilize
467 the primary DOC sources in both catchments, while the peak flow in SN was attained earlier.
468 Rainfall peak intensity in the Fitterizzi rain gauge (only 4.4 mm hr^{-1}) occurred in the same hour
469 as the rainfall peak in SN. However, this rain gauge is not within the SN catchment; hence some
470 rainfall features in this catchment, like the exact amount and timing, could have been missed.

471 Figs. 9e-f show a summer event (15.07.2019) for FIT, with a negative HI value (-0.26)
472 and significantly high DOC concentration. This event was characterized by a higher rainfall
473 amount than the previous case (32.6 mm hr^{-1} two hours before the peak flow, 8.6 mm hr^{-1} one
474 hour before and 15.8 mm hr^{-1} at the peak flow time). The suddenly increased hydraulic
475 connection in the river network given by this typical summer rain shower following a dry period
476 contributed to higher DOC concentration values in the falling limb.

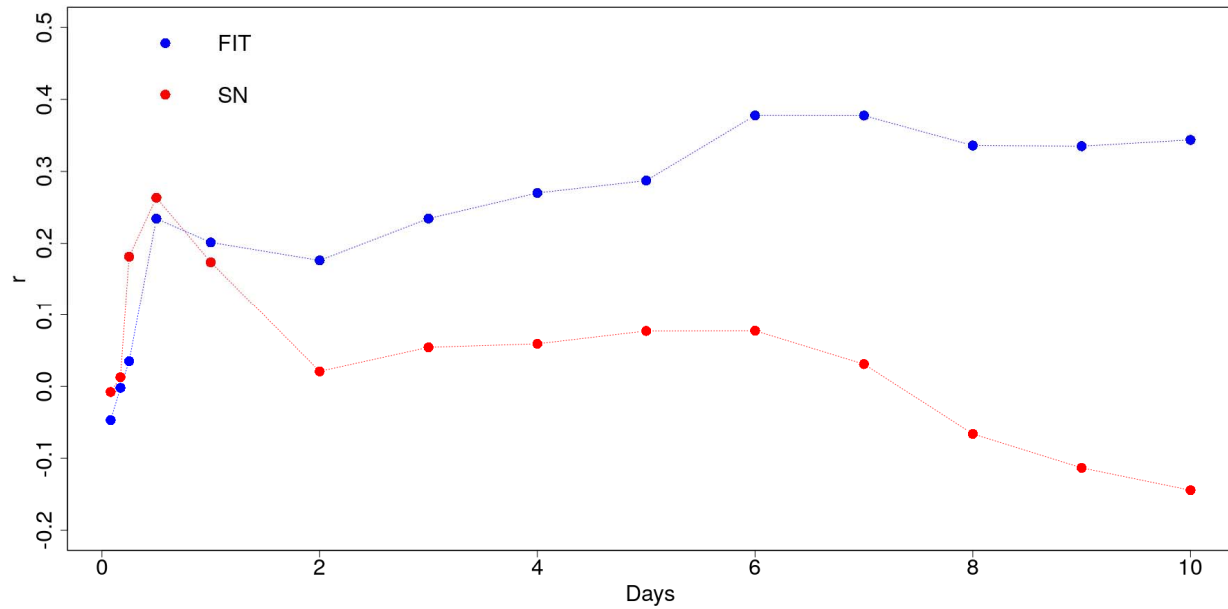
477 Finally, an event in SN with a positive HI value ($+0.27$) is shown (Figs. 9g-h). This event
478 occurred at the end of the winter (wet) period (20.03.2021), concatenating two consecutive
479 smaller events with clockwise evolution (Figure 9h). Interestingly, discharge was lower and
480 DOC concentration higher in the first event, consistently with the assumption that, for positive
481 HI values, the export processes are source-limited. In this case, rainfall intensity was low
482 (maximum 3.8 mm hr^{-1} at the Fitterizzi gauge station).



483

484 **Figure 9.** DOC concentrations and hydrographs and corresponding DOC–Q hysteresis during the
 485 events.

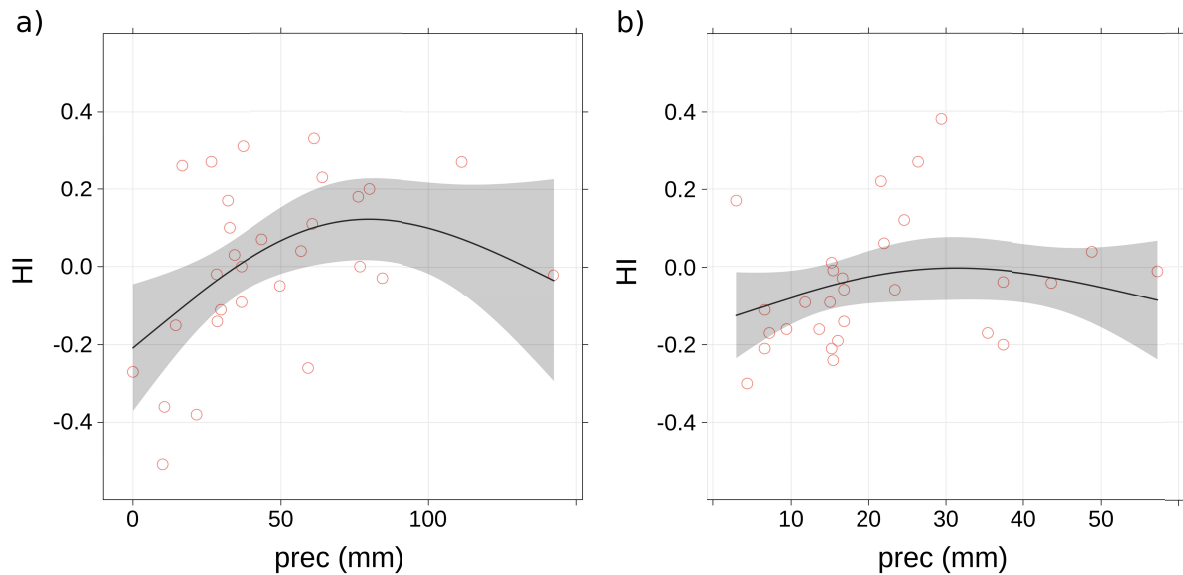
486 The higher correlation of HI with discharges in FIT and the more pronounced seasonality
 487 suggests that its variability can be partially explained by focusing on the antecedent weather
 488 conditions, influencing soil moisture and hydraulic connectivity. On the other hand, it can be
 489 tested if similar mechanisms were activated even at SN despite the lower correlation with
 490 discharge. Figure 10 shows the HI correlation with the precipitation accumulated over different
 491 time intervals, ranging from two hours to ten days before the discharge peak value. For both SN
 492 and FIT, a relative correlation peak was found for approximately 0.5 days of rainfall
 493 accumulation. After that, SN correlation decreased, while HI variability in FIT was more clearly
 494 explained by precipitation accumulated in the previous 6 to 7 days, up to $r = 0.38$ ($p < 0.001$).
 495 The lower correlation of SN with more extended accumulation periods can be explained by its
 496 smaller extent (hence, faster response to storm events) and the relatively higher contribution of
 497 groundwater to its discharge. On the other hand, network connectivity in FIT looks more
 498 sensitive to the precipitation accumulated over a longer time interval. However, r values were
 499 low overall.



500

501 **Figure 10.** HI correlation with precipitation accumulated in different time intervals (FIT and
502 SN).

503 The scatter plots of HI versus accumulated precipitation for the most highly correlated time
504 intervals (i.e., 6 days for FIT and 0.5 days for SN; Fig. 11) highlight the non-linear nature of the
505 correlation. Scattered points were interpolated through generalized additive models (GAMs,
506 Hastie and Tibshirani, 1986; 1990), which are smooth, nonparametric functions. Especially in
507 FIT (Figure 11a), GAMs highlighted the non-linear relation between HI and antecedent
508 precipitation. In general, for low accumulated precipitation values, DOC export was transport-
509 limited ($HI < 0$). Then, for higher accumulation values, meaning continuous (not necessarily
510 intense) precipitation in the considered interval, DOC sources tended to be flushed, and the
511 process became source-limited ($HI > 0$). Nevertheless, when accumulated precipitation was high
512 enough, it could mobilize other DOC sources, and the process tended to return transport-limited.
513 The event with the highest antecedent 6-day rainfall in FIT started on 25.01.2021 after several
514 other events had just happened. Indeed, the C-Q graph of this event (not shown) includes more
515 than one loop and is characterized as complex, according to Rose et al. (2018). The relation
516 between antecedent precipitation and hysteresis described for FIT is much more roughly
517 sketched out in the smaller SN catchment (Figure 11b), for which a smaller accumulation
518 interval was also considered.



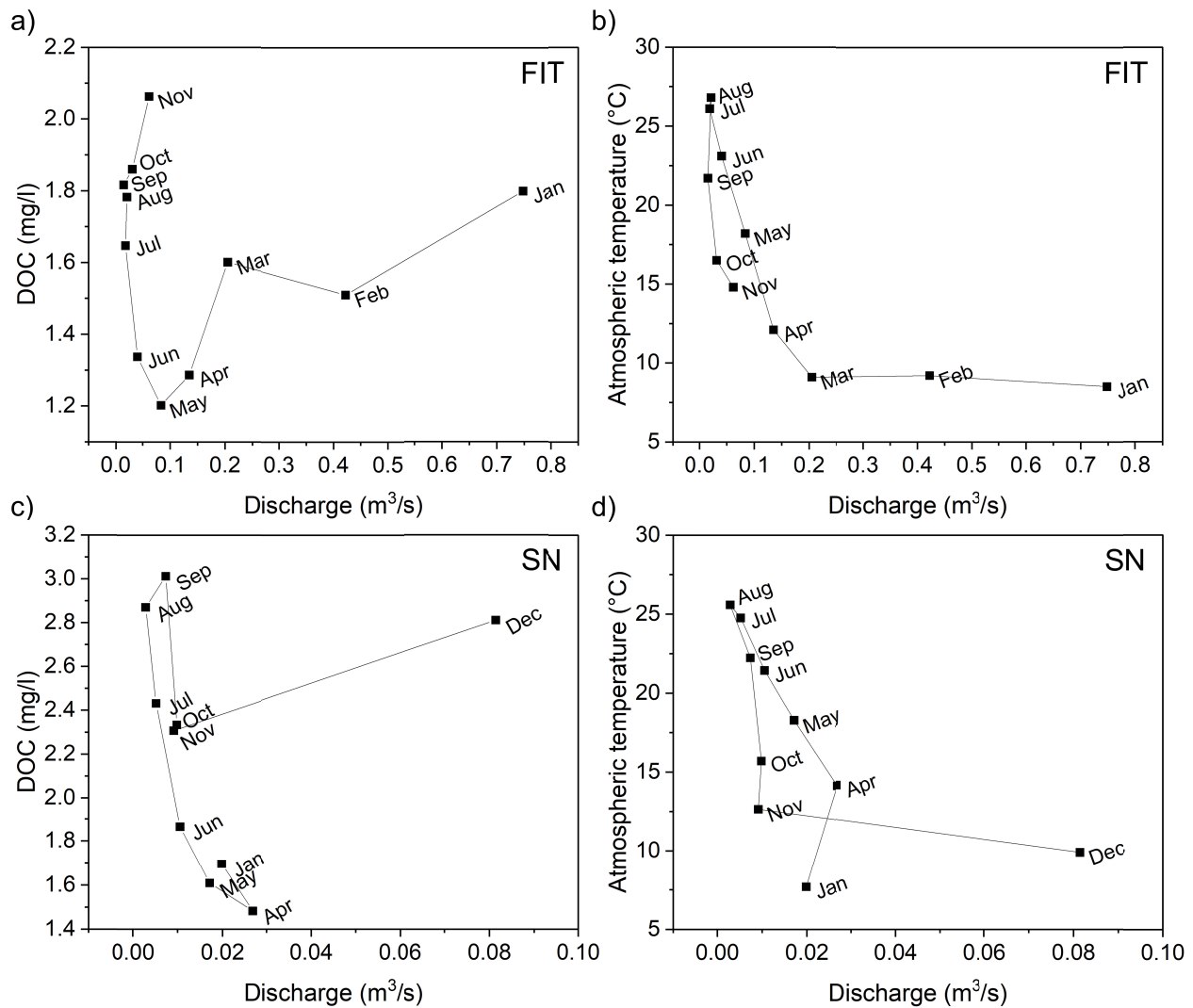
519

520 **Figure 11.** HI vs accumulated precipitation: a) FIT (6-day precipitation); b) SN (0.5-day
 521 precipitation).

522

523 4 Discussion

524 The seasonal pattern observed for DOC concentration in both sites (Figures 4 and 5)
 525 agrees with other studies that reported freshwaters DOC concentration peaking in autumn. In
 526 most cases, this seasonality is dependent on discharge (negative correlation), leading to
 527 clockwise hysteretic loops with respect to seasons due to lower DOC concentration in
 528 winter/spring and higher concentration in summer/autumn periods (Mulholland and Hill, 1997;
 529 Aubert et al., 2013; Dawson et al., 2008; Fovet et al., 2018). Figures 12a and 12c show the
 530 seasonal hysteretic cycles in the Q-C plane for Fitterizzi and San Nicola. Data refer to the years
 531 2021 and 2020, respectively, for which an almost complete series of data across the entire year
 532 were available. They confirm the expected pattern for the two sites under investigation, even
 533 though an anticipated DOC peak occurred in San Nicola, where the max DOC concentration was
 534 observed in late summer/early autumn.



535

536 **Figure 12.** Mean monthly concentrations of a), c) DOC and b), d) mean monthly atmospheric
 537 temperature plotted against mean monthly specific discharge for a), b) Fitterizzi (2021), and c),
 538 d) San Nicola (2020).

539

540 Intra-annual hysteretic loops in the Q-C plane reflect seasonality in the catchment
 541 streamflow dynamics and in-stream variation in the rate of net nutrient release and uptake.
 542 Therefore, they may show a site-dependent behaviour (Mulholland and Hill, 1997; Brooks et al.,
 543 1999; Dawson et al., 2001; Dawson et al., 2008; Aubert et al., 2013), as partially confirmed by
 544 our dataset. Differences may be explained through the unlike contribution of the dominant
 545 hydrologic pathway and in-stream processes in the two sites. Figures 12b and 12d show the
 546 corresponding hysteretic loops for the monthly mean atmospheric temperature, highlighting
 547 counterclockwise patterns to discharge for both locations. The peak temperature lagged about
 548 one month behind DOC in SN, while there was a larger inertia in the broader and lower elevation
 549 FIT catchment. Temperature is a critical hydro-climatic parameter affecting the seasonal pattern
 550 of stream water chemistry. Thus, it can be eventually used as an alternative to discharge to
 551 understand the intra-annual variability of water quality (Aubert et al., 2013). DOC and

552 temperature were positively correlated in both sites. Though, this correlation was more
553 significant in the San Nicola site, an instance which may explain the differences in the earlier
554 monthly DOC concentration peak observed in San Nicola.

555 The baseflow carries a relatively low amount of DOC, primarily mobilized by individual
556 storms. In agreement with previous studies, DOC peaks were observed during flood events
557 (Vaughan et al., 2017, Rose et al., 2018, Blaurock et al., 2021), when significant DOC
558 enhancement could be measured. As an example, Fovet et al. (2018) recorded an increase
559 $\Delta C = 5 \pm 4 \text{ mg C l}^{-1}$ compared to a concentration of $\text{DOC} < 1 \text{ mg C l}^{-1}$ during baseflow,
560 Blaurock et al. (2021) observed peaks of 10.2-18.6 mg l^{-1} and 8.5-16.9 mg l^{-1} for two sites in
561 comparison to a concentration of 2-3 mg l^{-1} during the baseflow.

562 This case study confirms the influence of the topography on the mechanism of DOC
563 mobilization and export during storms. Similarly to the catchment located in southeastern
564 Germany and analyzed by Blaurock et al. (2021), the DOC was monitored in two different sub-
565 catchments situated in an upper position with steep slopes and in a lower and flatter site. While
566 during the background periods, the DOC concentration was higher in the upstream sub-
567 catchment (i.e., SN), greater concentrations were recorded in the downstream site during the
568 storm events. The DOC average values in response to storm events confirm the results found by
569 Blaurock et al. (2021). They found average values for the 4 events reported equal 3.88 mg l^{-1} and
570 1.75 mg l^{-1} in the lower and upper sub-catchment, respectively. They correlated this behaviour to
571 topography, highlighting that saturated soils are needed in flatter areas to allow efficient lateral
572 water transport through DOC-rich soil layers towards the active river network. Moreover, like in
573 Blaurock et al. (2021), DOC mobilization was generally delayed in the flat lower catchment, as
574 confirmed by the slighter decrease after the peak and hysteretic loops wider than the upper
575 catchment (larger absolute values of HI in 13 cases out of the 19 simultaneous events).

576 In literature test areas, there is a prevalence of counterclockwise loops (negative values
577 of HI) for DOC hysteresis (e.g., 51 counterclockwise compared to only 3 clearly clockwise and
578 46 complex events in Rose et al., 2018; 6 cases out of 8 counterclockwise in Blaurock et al.,
579 2021). Instead, the flushing index FI is mainly positive (Vaughan et al., 2017). In this study, the
580 negative HI values were 21 over 29 and 13 over 29 for SN and FIT, respectively, while negative
581 FI values were only 5 out of 29 for SN and were undetected in FIT. The clockwise loop is likely
582 linked to the total catchment wetness seasonal pattern. Indeed, during or immediately after the
583 end of the wet season, when the catchment water storage is high, the hillslope-channel
584 hydrological connections are favoured compared to other periods, as shown by previous studies
585 in the catchment (Senatore et al., 2021; Micieli et al., 2022). Therefore the DOC peak anticipates
586 the discharge peak describing a clockwise hysteresis. This seasonal dependence of hysteresis is
587 also in line with the results of Fovet et al. (2018). They showed clockwise hysteresis for 62% of
588 events at a high flow period typical of the wet season in a Brittany, Western France catchment.

589 Finally, the study of the correlation between catchment wetness conditions and hysteresis
590 direction was already addressed. Blaurock et al. (2021) found a positive correlation with the
591 rainfall accumulated 14 days before the event started. Our analysis based on a variable
592 accumulation time window confirmed such influence and highlighted different process timings
593 depending on the catchment's size and other features. In larger, flatter catchments, complete
594 hydraulic activation generally requires extended periods. Nevertheless, also precipitation
595 intensity and amount count. We demonstrated that by expanding the analysis to high

596 precipitation amounts, a non-linear correlation arises, given by the connection of new DOC
597 sources far from the stream.

598 **5 Conclusions**

599 This study presented the results of a long-term monitoring campaign to unveil space and
600 time DOC dynamics in a Mediterranean headwater catchment, relating them to meteorological
601 and hydrological drivers. The different DOC dynamics observed in two nested sites were linked
602 to spatially heterogeneous catchment properties (extent, orographic features, land uses). Two
603 multi-parameter sondes were used to achieve that aim, and high-resolution continuous timeseries
604 of several biogeochemical parameters were obtained.

605 The analysis relied on an original correction method, requiring water temperature and
606 turbidity measurements to convert the observed fDOM into DOC values. Then, analyses
607 performed at seasonal and storm event timescales provided several insights into DOC
608 mobilization and export processes:

- 609 – At the seasonal scale, univariate and multivariate statistical analysis confirmed the climate
610 (seasonal) control on DOC production, with background concentrations increasing in hot
611 and dry summer months due to the combined effect of enhanced photocatalytic degradation
612 and reduced discharge in the channels;
- 613 – Comparison of DOC concentrations taken simultaneously over 91 non-rainy days led to
614 slightly higher values in the forested upstream catchment, having steeper topography and,
615 of course, smaller streamflow;
- 616 – However, observations made clear the importance of the hydrological regulation of DOC
617 export, significantly activated by high-flow events, with discharge above Q10 being
618 associated with 69% of the total yield in the upstream and 79% in the downstream site;
- 619 – Also, the increased hillslope-channel connectivity all over the downstream catchment
620 triggered by hydrological processes overturned the results of the seasonal background
621 analysis, with DOC concentration higher in the downstream site considering the 3760
622 simultaneous observations at the hourly time scale;
- 623 – DOC sources proved to be plentiful in the zones contributing to the catchment's fast
624 response in both sites, being able to increase concentration during almost all the storm
625 events. Instead, the limiting factor of DOC export processes varied by season and location.
626 In the steep upstream catchment with accentuated spatial intermittency, generally, such
627 processes were transport-limited, while in the downstream catchment, more source-limited
628 processes were observed;
- 629 – Therefore, the hysteresis index was more positively correlated to antecedent precipitation
630 in the downstream catchment. However, such correlation was not linear since new DOC
631 sources were activated with exceptionally high accumulated rainfall values, and the
632 process tended to be transport-limited again.

633 Overall, the study demonstrated the importance of high-resolution measurements to
634 explain DOC dynamics at multiple time scales with a quantitative approach. However, though
635 supported by laboratory measurements, the on-site recording showed some inherent weaknesses,
636 primarily when high discharge was associated with high turbidity values, requiring the statistical

637 retrieval of DOC peak values. Such a drawback can be partially overcome with increased on-site
 638 discrete automatic sampling during storm events and subsequent laboratory analysis. One of the
 639 further developments of the research goes towards this direction. Furthermore, it will be
 640 necessary to focus more on the processes' scaling properties, taking advantage of both the
 641 measurements in this and other sites, to support modelling approaches and contribute to a better
 642 understanding of the global carbon cycle.

643 **Acknowledgements, Samples, and Data**

644 We thank the “Centro Funzionale Multirischi” of the Calabrian Regional Agency for the
 645 Protection of the Environment for providing the observed meteorological dataset.

646 This study was supported by the European Research Council (ERC) DyNET project funded
 647 through the European Community's Horizon 2020 - Excellent Science - Programme (grant
 648 agreement H2020-EU.1.1.-770999).

649 Weather data are delivered, upon request, by the “Centro Funzionale Multirischi – ARPACAL”
 650 (<http://www.cfd.calabria.it>). The experimental data collected for this study are available at
 651 Senatore et al. (2022b).
 652

653 **References**

- 654 Ahmadi, B., Ahmadalipour, A., & Moradkhani, H. (2019). Hydrological drought persistence and
 655 recovery over the CONUS: a multi-stage framework considering water quantity and
 656 quality. *Water Research*, 150, 97–110. <https://doi.org/10.1016/j.watres.2018.11.052>
- 657 Aitkenhead-Peterson, J. A., Smart, R. P., Aitkenhead, M. J., Cresser, M. S., & McDowell, W. H.
 658 (2007). Spatial and temporal variation of dissolved organic carbon export from gauged
 659 and ungauged watersheds of Dee Valley, Scotland: Effect of land cover and C V N,
 660 *Water Resource Research*, 43, W05442. <https://doi.org/10.1029/2006WR004999>
- 661 Aubert, A. H., Gascuel-Oudou, C., & Merot, P. (2013). Annual hysteresis of water quality: A
 662 method to analyse the effect of intra and inter-annual climatic conditions. *Journal of*
 663 *Hydrology*, 478, 29–39. <http://dx.doi.org/10.1016/j.jhydrol.2012.11.027>
- 664 Basu, N.B., Destouni, G., Jawitz, J.W., Thompson, S.E., Loukinova, N.V., Darracq, A., Zanardo
 665 S., et al. (2010). Nutrient loads exported from managed catchments reveal emergent
 666 biogeochemical stationarity. *Geophysical Research Letters*, 37 (23), L23404.
 667 <https://doi.org/10.1029/2010GL045168>
- 668 Bengtson, P., & Bengtsson, G. (2007). Rapid turnover of DOC in temperate forests accounts for
 669 increased CO₂ production at elevated temperatures. *Ecology Letters*, 10 (9), 783–790.
 670 <https://doi.org/10.1111/j.1461-0248.2007.01072.x>
- 671 Bertuzzo, E., Helton, A.M., Hall, R.O., & Battin, T.J. (2017). Scaling of dissolved organic
 672 carbon removal in river networks. *Advances in Water Resources*, 110, 136-146.
 673 <https://doi.org/10.1016/j.advwatres.2017.10.009>
- 674 Blaurock, K., Beudert, B., Gilfedder, B. S., Fleckenstein, J. H., Peiffer, S., & Hopp, L. (2021).
 675 Low hydrological connectivity after summer drought inhibits DOC export in a forested

- 676 headwater catchment. *Hydrology and Earth System Sciences*, 25(9), 5133-5151.
 677 <https://doi.org/10.5194/hess-25-5133-2021>
- 678 Botter, G., Vingiani, F., Senatore A., Jensen C., Weiler M., McGuire K., et al. (2021).
 679 Hierarchical climate-driven dynamics of the active channel length in temporary streams.
 680 *Scientific Reports*, 11, 21503. <https://doi:10.1038/s41598-021-00922-2>
- 681 Brooks P. D., McKnight D. M., & Bencala K. E. (1999). The relationship between soil
 682 heterotrophic activity, soil dissolved organic carbon (DOC) leachate, and catchment-scale
 683 DOC export in headwater catchments. *Water Resource Research*, 35:1895–1902.
 684 <https://doi:10.1029/1998WR900125>
- 685 Butman, D., & Raymond, P. A. (2011). Significant efflux of carbon dioxide from streams and
 686 rivers in the United States. *Nature Geoscience*, 4(12), 839– 842.
 687 <https://doi.org/10.1038/ngeo1294>
- 688 Butturini, A., Alvarez, M., Bernal, S., Vazquez, E., & Sabater F. (2008), Diversity and temporal
 689 sequences of forms of DOC and NO₃-discharge responses in an intermittent stream:
 690 Predictable or random succession?, *Journal of Geophysical Research*, 113, G03016,
 691 <https://doi.org/10.1029/2008JG000721>
- 692 Chaplot, V. & Mutema, M. (2021). Sources and main controls of dissolved organic and inorganic
 693 carbon in river basins: A worldwide meta-analysis. *Journal of Hydrology*, 603, 126941.
 694 <https://doi.org/10.1016/j.jhydrol.2021.126941>
- 695 Chen, S., Zhong, J., Li, C., Liu, J., Wang, W., Xu, S., & Li, S. L. (2021), Coupled effects of
 696 hydrology and temperature on temporal dynamics of dissolved carbon in the Min River,
 697 Tibetan Plateau. *Journal of Hydrology*, 593, 125641.
 698 <https://doi.org/10.1016/j.jhydrol.2020.125641>
- 699 Chorover, J., Derry, L.A., & McDowell, W.H., (2017). Concentration-discharge relations in the
 700 critical zone: Implications for resolving critical zone structure, function, and evolution.
 701 *Water Resources Research*, 53(11), 8654-8659. <https://doi.org/10.1002/2017WR021111>
- 702 Cole, J.J., Prairie, Y.T., Caraco, N.F., McDowell, W.H., Tranvik, L.J., Striegl, R.G., et al., AU
 703 (2007). Plumbing the global carbon cycle: Integrating inland waters into the terrestrial
 704 carbon budget. *Ecosystems*, 10, 171-184. <https://doi.org/10.1007/s10021-006-9013-8>
- 705 Dawson J.J.C., Billett M.F., & Hope D. (2001). Diurnal variations in the carbon chemistry of two
 706 acidic upland streams in northeast Scotland. *Freshwater Biology*, 46, 1309–1322.
 707 <https://doi:10.1046/j.1365-2427.2001.00751.x>.
- 708 Dawson J.J.C., Soulsby, C., Tetzlaff, D., Hrachowitz, M., Dunn S. M., & Malcolm, I. A., (2008).
 709 Influence of hydrology and seasonality on DOC exports from three contrasting upland
 710 catchments. *Biogeochemistry*, 90, 93–113. <https://doi.org/10.1007/s10533-008-9234-3>.
- 711 Downing B.D., Pellerin, B.A., Bergamaschi, B.A., Saraceno, J.F., & Kraus T.E.C. (2012).
 712 Seeing the light: The effects of particles, dissolved materials, and temperature on in situ
 713 measurements of DOM fluorescence in rivers and streams. *Limnology and*
 714 *Oceanography: Methods*, 10: 767-775. <https://doi.org/10.4319/lom.2012.10.767>
- 715 Exo User Manual, Advanced Water Quality Monitoring Platform, YSI, a Xylem brand. Yellow
 716 Springs, OH, US, 2020.

- 717 Fazekas, H.M., Wymore, A.S., & McDowell, W.H. (2020). Dissolved organic carbon and nitrate
 718 concentration-discharge behavior across scales: Land use, excursions, and
 719 misclassification. *Water Resources Research*, 56, e2019WR027028.
 720 <https://doi.org/10.1029/2019WR027028>
- 721 Fovet, O., Humbert, G., Dupas, R., Gascuel-Oudou, C., Gruau, G., Jaffrézic, A., et al. (2018),
 722 Seasonal variability of stream water quality response to storm events captured using high-
 723 frequency and multi-parameter data. *Journal of Hydrology*, 559, 282-293.
 724 <https://doi.org/10.1016/j.jhydrol.2018.02.040>
- 725 Freeman, C., Evans, C.D., Monteith, D.T., Reynolds, B., & Fenner, N., 2001. Export of organic
 726 carbon from peaty soils. *Nature*, 412, 785. <https://doi.org/10.1038/35090628>
- 727 Giesbrecht, I.J. W., Tank, S.E., Frazer, G.W., Hood, E., Gonzalez Arriola, S.G., Butman, D.E., et
 728 al. (2022). Watershed classification predicts streamflow regime and organic carbon
 729 dynamics in the Northeast Pacific Coastal Temperate Rainforest. *Global Biogeochemical*
 730 *Cycles*, 36, e2021GB007047. <https://doi.org/10.1029/2021GB007047>
- 731 Godsey, S.E., Kirchner, J.W., & Clow D.W. (2009). Concentration–discharge relationships
 732 reflect chemostatic characteristics of US catchments. *Hydrological Processes: An*
 733 *International Journal*, 23(13), pp.1844-1864. <https://doi.org/10.1002/hyp.7315>
- 734 Hastie, T., & Tibshirani, R. (1986). Generalized Additive Models, *Statistical Science*, Vol. 1, No
 735 3, 297-318.
- 736 Hastie, T., & Tibshirani, R. (1990). Generalized Additive Models, Chapman & Hall/CRC, New
 737 York/Boca Raton
- 738 Humbert, G., Jaffrezic, A., Fovet, O., Gruau, G., & Durand P. (2015), Dry season length and
 739 runoff control annual variability in stream DOC dynamics in a small, shallow
 740 groundwater-dominated agricultural watershed, *Water Resource Research*, 51, 7860–
 741 7877, <https://doi.org/10.1002/2015WR017336>
- 742 Jones, T.D., Chappell, N.A., & Tych, W. (2014). First dynamic model of dissolved organic
 743 carbon derived directly from high-frequency observations through contiguous storms.
 744 *Environmental science & technology*, 48(22), pp.13289-13297.
 745 <https://doi.org/10.1021/es503506m>
- 746 Koenig, L.E, Shattuck, M.D., Snyder, L.E., Potter, J.D., & McDowell, W.H. Deconstructing the
 747 effects of flow on DOC, nitrate, and major ion interactions using a high-frequency
 748 aquatic sensor network. *Water Resources Research*, 53, 10,655–10,673.
 749 <https://doi.org/10.1002/2017WR020739>
- 750 Ladson, A., Brown, R. Neal B. & Nathan, R. (2013). A standard approach to baseflow separation
 751 using the Lyne and Hollick filter. *Australasian Journal of Water Resources*, 17(1), pp.25-
 752 34. <https://doi.org/10.7158/13241583.2013.11465417>
- 753 Lloyd, C.E., Freer, J.E., Johnes, P.J., & Collins, A.L. (2016). Testing an improved index for
 754 analysing storm discharge–concentration hysteresis. *Hydrology and Earth System*
 755 *Sciences*, 20(2), pp.625-632. <https://doi.org/10.5194/hess-20-625-2016>
- 756 Lowe W.H., Likens G.E., & Power M.E. (2006). Linking scales in stream ecology. *Bioscience*,
 757 56(7):591–597. [https://doi.org/10.1641/0006-3568\(2006\)56\[591:LSISE\]2.0.CO;2](https://doi.org/10.1641/0006-3568(2006)56[591:LSISE]2.0.CO;2)

- 758 McGuire, K.J., Torgersen, C.E., Likens, G.E., Buso, D.C., Lowe, W.H., & Bailey, S.W. (2014).
759 Network analysis reveals multiscale controls on streamwater chemistry. *Proceedings of*
760 *the National Academy of Sciences*, 111 (19) 7030-7035.
761 <https://doi.org/10.1073/pnas.1404820111>
- 762 Mehring, A.S., Lowrance, R.R., Helton, A.M., Pringle, C.M., Thompson, A., Bosch, D.D., &
763 Vellidis, G. (2013). Interannual drought length governs dissolved organic carbon
764 dynamics in blackwater rivers of the western upper Suwannee River basin. *Journal of*
765 *Geophysical Research: Biogeosciences*, 118, 1636–1645.
766 <https://doi.org/10.1002/2013JG002415>
- 767 Mendicino, G., & Versace, P. (2007). Integrated Drought Watch System: A Case Study in
768 Southern Italy. *Water Resources Management*, 21:8, 21(8), 1409–1428.
769 <https://doi.org/10.1007/S11269-006-9091-6>
- 770 Micieli, M., Botter, G., Mendicino, G., & Senatore, A (2022). UAV Thermal Images for Water
771 Presence Detection in a Mediterranean Headwater Catchment. *Remote Sensing*, 14, 108.
772 <https://doi.org/10.3390/rs14010108>
- 773 Mistick, E., & Johnson, M.S. (2020). High-frequency analysis of dissolved organic carbon storm
774 responses in headwater streams of contrasting forest harvest history. *Journal of*
775 *Hydrology*, 590, p.125371. <https://doi.org/10.1016/j.jhydrol.2020.125371>
- 776 Monteith, D.T., Stoddard, J.L., Evans, C.D., de Wit, H.A., Forsius, M., Høgåsen, T., Wilander,
777 A., et al., (2007). Dissolved organic carbon trends resulting from changes in atmospheric
778 deposition chemistry. *Nature*, 540, 527–540. <https://doi.org/10.1038/nature06316>
- 779 Morison, M.Q., Higgins, S. N., Webster, K. L., Emilson, E. J. S., Yao, H., & Casson, N. J.
780 (2022), Spring coherence in dissolved organic carbon export dominates total coherence in
781 Boreal Shield forested catchments. *Environmental Research Letters*, 17, 014048.
782 <https://doi.org/10.1088/1748-9326/ac462f>
- 783 Mulholland, P.J., & Hill, W.R., 1997. Seasonal patterns in streamwater nutrient and dissolved
784 organic carbon concentrations: separating catchment flow path and in-stream effects.
785 *Water Resource Research*, 33 (6), 1297–1306. <https://doi.org/10.1029/97WR00490>
- 786 Musolff, A., Schmidt, C., Selle, B., & Fleckenstein, J. H. (2015). Catchment controls on solute
787 export. *Advances in Water Resources*, 86, 133–146.
788 <https://doi.org/10.1016/j.advwatres.2015.09.026>
- 789 Parr T.B., Inamdar S.P., & Miller M.J. (2019). Overlapping anthropogenic effects on hydrologic
790 and seasonal trends in DOC in a surface water dependent water utility. *Water Research*,
791 148, 407-415. <https://doi.org/10.1016/j.watres.2018.10.065>
- 792 Pellerin, B.A. & Bergamaschi B.A., (2014). Optical sensors for water quality. Lakeline, Spring,
793 *North American Lake Management Society*, pp.13-17
- 794 Rose, L.A., Karwan, D.L., & Godseyet, S.E. (2018). Concentration–discharge relationships
795 describe solute and sediment mobilization, reaction, and transport at event and longer
796 timescales. *Hydrological Processes*, 32(18), pp.2829-2844.
797 <https://doi.org/10.1002/hyp.13235>

- 798 Roulet, N. & Moore, T.R., (2006). Browning the waters. *Nature*, 444(7117), pp.283-284.
799 <https://doi.org/10.1038/444283a>
- 800 Rovelli, L., Attard, K. M., Heppell, C. M., Binley, A., Trimmer, M., & Glud, R. N. (2018).
801 Headwater gas exchange quantified from O₂ mass balances at the reach scale. *Limnology*
802 *and Oceanography: Methods*, 16(10), 696– 709. <https://doi.org/10.1002/lom3.10281>
- 803 Saraceno, J. F., Pellerin, B.A., Downing, B.D., Boss, E., Bachand, P.A.M. & Bergamaschi B.A.
804 (2009), High-frequency in situ optical measurements during a storm event: Assessing
805 relationships between dissolved organic matter, sediment concentrations, and hydrologic
806 processes, *Journal of Geophysical Research*, 114, G00F09,
807 <https://doi.org/10.1029/2009JG000989>
- 808 Seybold, E., Gold, A. J., Inamdar, S. P., Adair, C., Bowden, W. B., Vaughan, M. C. H., et al.
809 (2019). Influence of land use and hydrologic variability on seasonal dissolved organic
810 carbon and nitrate export: insights from a multiyear regional analysis for the northeastern
811 USA, *Biogeochemistry*, 146, 31–49, <https://doi.org/10.1007/s10533-019-00609-x>
- 812 Senatore, A., Micieli, M., Liotti, A., Durigetto, N., Mendicino, & G., Botter G. (2021).
813 Monitoring and Modeling Drainage Network Contraction and Dry Down in
814 Mediterranean Headwater Catchments. *Water Resources Research*, 57(6),
815 e2020WR028741. <https://doi.org/10.1029/2020WR028741>
- 816 Senatore, A., Fuoco, D., Maiolo, M., Mendicino, G., Smiatek, G., & Kunstmann, H. (2022a).
817 Evaluating the uncertainty of climate model structure and bias correction on the
818 hydrological impact of projected climate change in a Mediterranean catchment. *Journal*
819 *of Hydrology: Regional Studies*, 42, 101120.
820 <https://doi.org/10.1016/J.EJRH.2022.101120>
- 821 Senatore, A., Corrente, G.A., Argento, E.L., Castagna, J., Micieli, M., Mendicino, M., Beneduci,
822 A., & Botter, G. (2022b). Seasonal and storm event-based dynamics of dissolved organic
823 carbon (DOC) concentration in a Mediterranean headwater catchment – DATASET.
824 Retrieved from <https://researchdata.cab.unipd.it/id/eprint/801> doi:
825 10.25430/researchdata.cab.unipd.it.00000801
- 826 Shogren, A.J., Zarnetske, J.P., Abbott, B.W., Iannucci, F., Medvedeff, A., Cairns, S., et al.
827 (2021). Arctic concentration–discharge relationships for dissolved organic carbon and
828 nitrate vary with landscape and season. *Limnology and Oceanography*, 66, pp. S197-
829 S215. <https://doi.org/10.1002/lno.11682>
- 830 Snyder L., Potter, J.D., & McDowell W.H. (2018). An Evaluation of Nitrate, fDOM, and
831 Turbidity Sensors in New Hampshire Streams. *Water Resources Research*, 54, 2466-
832 2479. <https://doi.org/10.1002/2017WR020678>
- 833 Soares, A.R.A., Lapierre, J.F., Selvam, B.P., Lindström G., & Berggren M. (2019). Controls on
834 Dissolved Organic Carbon Bioreactivity in River Systems. *Scientific Reports*, 9:14897.
835 <https://doi.org/10.1038/s41598-019-50552-y>.
- 836 Song, X., Sidana L., Kun S., Yang G., & Xuefa W. (2021). Flux and source of dissolved
837 inorganic carbon in a headwater stream in a subtropical plantation catchment. *Journal of*
838 *Hydrology*, 600, 126511. <https://doi.org/10.1016/j.jhydrol.2021.126511>

- 839 Stumm, W. & Morgan, J.J. (1996) *Aquatic Chemistry, Chemical Equilibria and Rates in Natural*
 840 *Waters*. 3rd Edition, *John Wiley & Sons, Inc.*, New York. ISBN: 978-0-471-51185-4
- 841 Vaughan, M. C. H., Bowden, W. B., Shanley, J. B., Vermilyea, A., Sleeper, R., Gold, A. J. et al.
 842 (2017), High-frequency dissolved organic carbon and nitrate measurements reveal
 843 differences in storm hysteresis and loading in relation to land cover and seasonality,
 844 *Water Resource Research*, 53, 5345–5363. <https://doi.org/10.1002/2017WR020491>
- 845 Viza, A., Muñoz, I., Oliva F., & Menéndez M. (2022), Contrary effects of flow intermittence
 846 and land uses on organic matter decomposition in a Mediterranean river basin. *Science of*
 847 *The Total Environment*, 812, p.151424. <https://doi.org/10.1016/j.scitotenv.2021.151424>
- 848 Watras, C.J., Hanson, P.C., Stacy, T.L., Morrison, K.M., Mather, J., Hu, Y.-H., & Milewski P.
 849 (2011). A temperature compensation method for CDOM fluorescence sensors in
 850 freshwater. *Limnology and Oceanography: Methods*, 9: 296-301.
 851 <https://doi.org/10.4319/lom.2011.9.296>
- 852 Weiler, M. & McDonnell, J. J. (2006). Testing nutrient flushing hypotheses at the hillslope scale:
 853 A virtual experiment approach, *Journal of Hydrology*, 319, 339–356,
 854 <https://doi.org/10.1016/j.jhydrol.2005.06.040>
- 855 Werner, B. J., Musolff, A., Lechtenfeld, O. J., de Rooij, G. H., Oosterwoud, M. R., &
 856 Fleckenstein, J. H. (2019). High-frequency measurements explain quantity and quality of
 857 dissolved organic carbon mobilization in a headwater catchment. *Biogeosciences*, 16(22),
 858 pp.4497-4516. <https://doi.org/10.5194/bg-16-4497-2019>
- 859 Williams, G. P. (1989). Sediment concentration versus water discharge during single hydrologic
 860 events in rivers. *Journal of Hydrology*, 111(1–4), 89–106. [https://doi.org/10.1016/0022-](https://doi.org/10.1016/0022-1694(89)90254-0)
 861 [1694\(89\)90254-0](https://doi.org/10.1016/0022-1694(89)90254-0)
- 862 Worrall, F. & Burt, T.P. (2007). Trends in DOC concentration in Great Britain. *Journal of*
 863 *Hydrology*, 346, 81-92, <https://doi.org/10.1016/j.jhydrol.2007.08.021>
- 864 Wu, J., Yao, H., Yuan, X., & Lin, B. (2022). Dissolved organic carbon response to hydrological
 865 drought characteristics: Based on long-term measurements of headwater streams. *Water*
 866 *Research*, 215, p.118252. <https://doi.org/10.1016/j.watres.2022.118252>
- 867 Zhong, J., Li, S.L., Ibarra, D.E., Ding, H., & Liu, C.Q. (2020). Solute Production and Transport
 868 Processes in Chinese Monsoonal Rivers: Implications for Global Climate Change. *Global*
 869 *Biogeochemical Cycles*. <https://doi.org/10.1029/2020gb006541>